AD NUMBER: AD0874646

LIMITATION CHANGES

TO:

Approved for public release; distribution is unlimited.

FROM:

Distribution authorized to US Government Agencies only; Export Control; Other requests should be referred to Air Force Institute of Technology, Wright-Patterson AFB, OH, 45433.

AUTHORITY

Per AFIT memo dtd 22 Jul 1971

AIR FORCE INSTITUTE OF TECHNOLOGY

AIR UNIVERSITY
UNITED STATES AIR FORCE

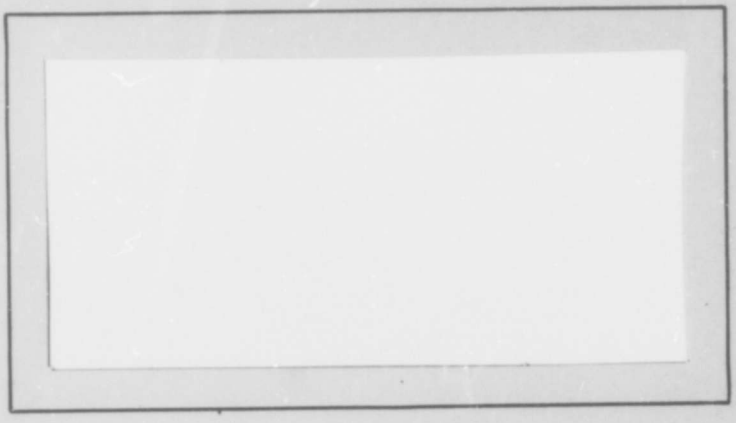

SCHOOL OF ENGINEERING

WRIGHT-PATTERSON AIR FORCE BASE, OHIO

GSP/PH/70-6

A TEST OF THE SYNCHROTRON EXPANDING SOURCE MODEL OF QUASI-STELLAR RADIO SOURCE VARIATIONS

THESIS

GSP/PH/70-6 Gordon Derossi
Captain USAF

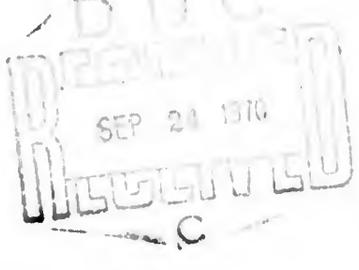

GSP/PH/70-6

A TEST OF THE SYNCHROTRON EXPANDING SOURCE MODEL OF QUASI-STELLAR RADIO SOURCE VARIATIONS

THESIS

Presented to the Faculty of the School of Engineering of
the Air Force Institute of Technology
Air University
in Partial Fulfillment of the
Requirements for the Degree of
Master of Science

by

Gordon Derossi, B.S.A.E.
Captain USAF

Graduate Space Physics Engineering

June 1970

Preface

This thesis represents the results of my attempt to test the validity of a mathematical model proposed to explain the observed radio variations of quasi-stellar objects. To do this I compared the actual variations observed from four quasi-stellar objects with the variations predicted by the model. Not only was the model successful in over 85% of the cases, but it lead me to discover two possible crossovers in time between the generation of two bursts of radio energy and their subsequent observation on earth.

I wish to take this opportunity to thank Col. Donald L. Evans for giving me the opportunity to work at the Space and Missile Systems Organization (AFSC) and the Aerospace Corporation. I also wish to thank all the people at The Aerospace Corporation for their support. I especially want to thank Dr. Eugene Epstein, who not only suggested this theses, but also supplied the encouragement and advice without which this paper could not have been completed. I also wish to express my appreciation to all those who supplied me with the data necessary to my analysis. Finally, I thank my wife for her patience and diligent effort in typing this entire report.

Gordon Derossi

Contents

Contents

List of Figures

List of Figures

List of Tables

Abstract

The validity of the synchrotron expanding source model for quasars as proposed by Shklovskii, Kellerman, and van der Laan is tested, using observations of the radio emission from four quasi-stellar radio sources. The time dependence of the recorded variations of radio emission in the range from 3.3 mm to approximately 6 cm, taken during the period from 1965 to late 1969 from QSS 3C84, 3C120, 3C273 and 3C454.3 is compared to the time dependence of the variations predicted by the proposed model. Correlation between the observed variations and the predicted variations is excellent in over 85% of the cases tested.

I. Introduction

Temporal variations in observed radiation may arise from intrinsic variations within the radiating region or from properties of the medium between the source and the observer. The medium through which the energy passes may cause absorption, reflection or refraction of the radiation. This paper compares observed radio variations from four extragalactic objects to the theoretical variations of a model proposed to explain them.

Until 1965 the only observed radio variability believed to come from an object outside the solar system was from the intense supernova remnant Cassiopeia A. It had been generally assumed that, apart from occasional supernova explosions or outbursts of previously detected optically variable stars in relatively nearby galaxies, no significant changes in the radio intensity of extragalactic objects should occur on a time scale shorter than the life span of a human observer. The large linear dimensions of the objects seemed to preclude radio variations on a short time scale. Specifically, if the emission is due to synchrotron radiation, it was considered unlikely that the time required to accelerate particles to speeds close to that of light, i.e., to relativistic energies or their subsequent decay by synchrotron radiation losses could be much less than about 10^6 years (Ref.19:418).

The discovery, in 1965, of remarkable intense changes

in the radio flux of a number of discrete quasi-stellar radio sources, (QSS), seemed to imply that enormous amounts of energy are generated in extremely small volumes of space. A quasi-stellar radio source is a celestial object that resembles a star but emits unusually bright blue and ultraviolet light and intense radio waves, and usually has a very large red-shift. A discrete source is one that is distinct or separate. Such a source can be either a point source, a localized source, or an extended source. A point source is an idealization defined as one which subtends an infinitesimal solid angle. A localized source is a discrete source of small but finite angular extent. An extended source is larger. The distinction between localized and extended is arbitrary, but it has been common practice to identify sources with diameters less than one degree as localized. All of the known QSS are of extremely small angular size, i.e., $\ll 1'$ (ref.19:421) and are regarded, in this paper, as point sources.

This discovery was not made before 1965 partly because no one thought to look for this type phenomena. The possibility that the variations are caused by properties of the medium through which the radiation passes has been ruled out by the results from extensive observations and comparisons of observed signals from QSS that are separated by only a very small angle. No systematic variations were observed. The variations are, therefore, produced in or at the sources.

The question, then, is, what is the physical mechanism that produces the observed time variations in the intensity of emitted radiation? It has been suggested by Shklovskii (Ref.37:234), Kellerman (Ref.17:621), and van der Laan (Ref.47:1131) that the varying components of the radiation from QSS are due to sources of Synchrotron radiation. Other possible mechanisms for the production of variable radiation are: plasma oscillation, Cerenkov radiation, and thermal free-free radiation. These have been shown to be much less likely than the synchrotron hypothesis (Ref.42:689-690).

At any one instant of time, the observed radio spectrum of a QSS has a cutoff at a particular frequency, i.e., the intensity is much less at frequencies below this critical frequency. As time passes, the critical frequency decreases. The proposed model accounts for this by assuming the source is radially expanding, emitting synchrotron radiation and is synchrotron self-absorbed below some critical frequency. Synchrotron self-absorption occurs when the optical depth at the frequencies being absorbed is very large. A photon produced by one spiralling electron is reabsorbed by another electron before it travels far enough to leave the source. The target electron then reradiates isotropically at lower frequencies. In other words, the source is initially optically thick, but as it expands, becomes optically thin at progressively lower frequencies. It has been shown (Ref.40:344) that other

possibilities for the cutoff in the spectrum, such as free-free absorption, are very unlikely in these sources and that synchrotron self-absorption provides the best explanation for the cutoff.

The purpose of this paper is to determine if the observed flux density variations of the quasi-stellar radio sources 3C273, 3C454.3 and the related radio galaxies 3C84 and 3C120 are compatible with the predictions based on the expanding source models as proposed by Shklovskii, Kellerman and van der Laan.

For any discrete source the integral of the spectral intensity over the source yields the total source flux density:

$$S = \int I\,(r,\theta,\phi)\; d\Omega \qquad (1)$$

where S = flux density of the source, watts $m^{-2}Hz^{-1}$

$I(r,\theta,\phi)$ = intensity as a function of position over the source, watts $m^{-2}Hz^{-1}\,rad^{-2}$

$d\Omega$ = element of solid angle, rad^2

The flux density of most celestial radio sources is of the order of 10^{-26} watts $m^{-2}Hz^{-1}$ and this quantity is commonly called one flux unit.

It will be assumed that synchrotron radiation is the only energy loss mechanism, apart from the energy that goes into the expansion. The attitude here is to admit the presently mysterious nature of the initial events giving rise to the relativistic electrons. This investigation includes analysis of frequencies from 750 MHz to

90 GHz; however, no examination of the polarization of the received signals is made.

The equipment and methods used to obtain the 90-GHz data are presented in Section II. These are representative of the equipment and methods used at the other frequencies. Next, the expanding source model is explained, including the derivation of the equations predicting the time dependence of the radio spectrum as the source evolves. The relationships between the flux density and wavelength are also derived from the model an it is shown how variations observed at one wavelength may be used to predict the behavior at any other wavelength.

Radio frequency data for the QSS 3C273, 3C454.3 and the related radio galaxies 3C84 and 3C 120 from a wavelength of 3.3 mm to approximately 11 cm is compiled for the period from 1965 to late 1969. Since the proposed model deals only with the variable part of a radio source output, the observed data is first adjusted to separate the varying components from the quiescent components. Next, the evaluation of each adequately observed outburst of each object is compared to the behavior predicted by the model. Values for T_o, the time of initiation of each event, γ, the index of the electron energy distribution, and β, an acceleration parameter, are found for each event.

The conclusions are limited to whether or not the model satisfactorily explains the observed variations.

In the case where the data is not consistent with the model, only qualitative attempts are made to alter the model.

II. Observations

Observations of quasi-stellar radio sources (QSS) at 90 GHz (3.3 mm) were made with the radio telescope of the Space Radio Systems Facility of The Aerospace Corporation at El Segundo, California. Data at other wavelengths was obtained from published articles (Ref. 14:L16, 25:L82, 26:7, 27:294-295, 32:956-963, 33:635) and, for the most recent data, directly from other active investigators (Ref.15, 24, 31, and 49). A program of monitoring QSS at 3.3 mm has been under way at Aerospace since April, 1965. The equipment, observing procedures and data reduction methods used to obtain the 3.3-mm information are, in general, representative of widely used radio astronomical techniques. No attempt will be made here to describe the acquisition methods at wavelengths other than 3.3 mm.

Equipment

The radio telescope equipment consists of four basic units. These are the antenna, the hydraulic servo system, the computer, and the radiometric receiver and temperature calibration standard. (Fig. 1).

Antenna. The antenna is an equatorially mounted, 15 foot diameter parabolic Cassegrain with a gain of 70.3 db at 90 GHz (Fig. 2). Two feed horns are mounted at the focus of the antenna, producing two patterns of reception, or "beams". The two beams have widths of 3.0 minutes of arc between half power points and are separated by 25 minutes of arc in hour angle.

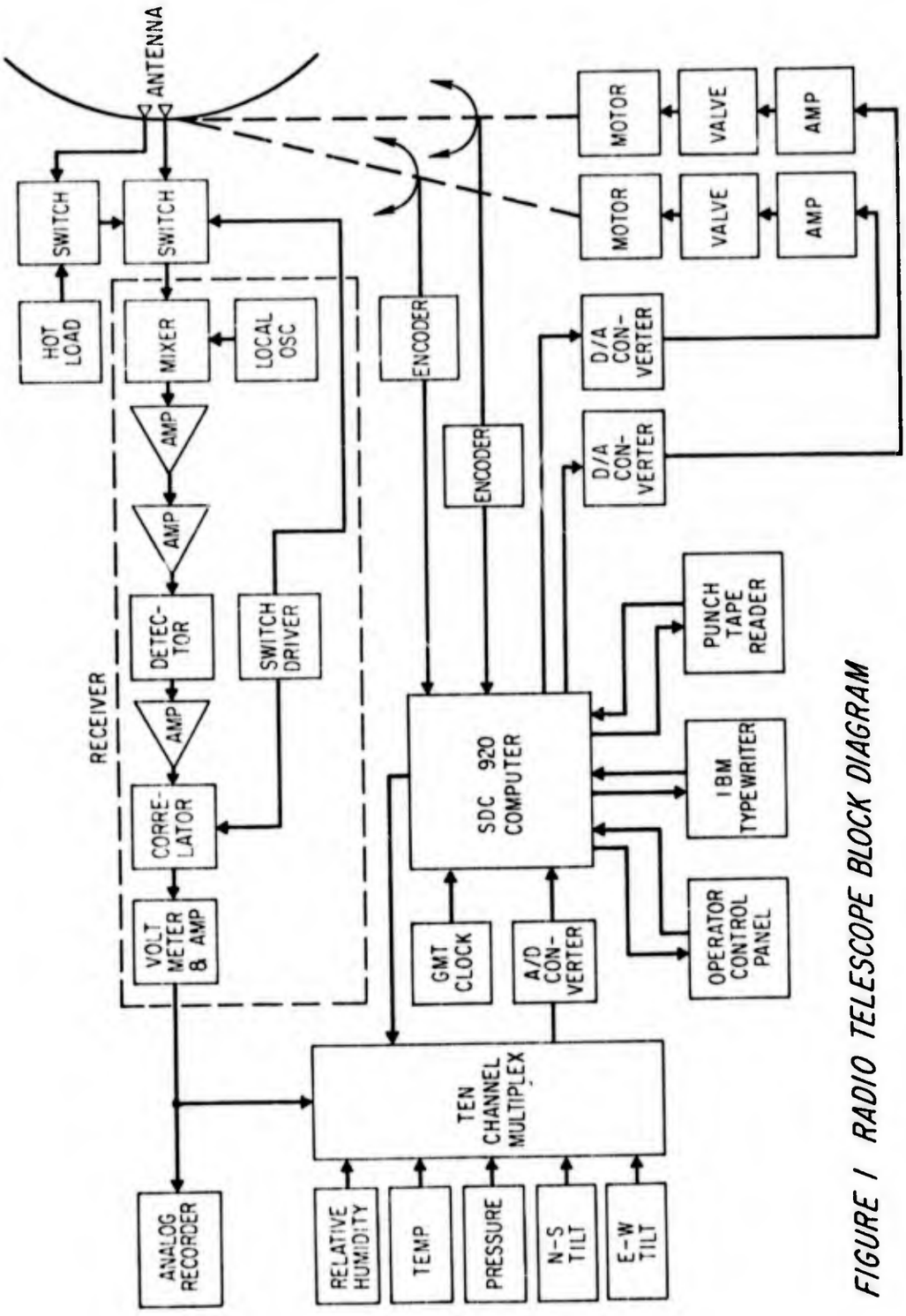

FIGURE I RADIO TELESCOPE BLOCK DIAGRAM

Figure 2 Radio Telescope

Hydraulic System. The hydraulic servo system provides antenna positioning, tracking and control. The servo system is capable of tracking with rates from 0.001 to 3.0 degrees per second. Angular positions of the axes in hour angle and declination is determined by 20-bit (1.24 arc-seconds/bit) Datex Corporation shaft angle encoders.

Computer. A Scientific Data Systems (SDS) 920 computer, programmed with ACP1L1, a locally written program, is used as a general purpose, on-line computer. It provides antenna position and tracking control and real time data reduction. The computer continually samples, on a

priority interrupt basis, Universal Time, shaft angle positions, meteorological sensors, and building tilt transducers. Subroutine programs compute this data in real-time to provide local sidereal time and modification in antenna position to correct for atmospheric refraction, building tilt, axis misalignment, and calibrated structural flexure of the antenna and the mount.

An integral part of the computer is an SDS AD 10-14 analog-to-digital converter. The sample rate used in these observations is ten samples per second.

Receiver. The receiver is of the Dicke switching type. The crystal mixer input is switched at a 500-Hz rate between the two beams. A klystron local oscillator produces an intermediate frequency of 3 GHz with an IF bandwidth of 1.5 GHz. The receiver has an overall output noise fluctuation of $\approx 0.06^{\circ}K$, for an RC time constant of 1 second.

A hot-load resistor provides the calibration temperature standard. The resistor temperature is approximately $357^{\circ}K$, and is monitored with a thermocouple and bridge to an accuracy of $\pm$ 0.1%.

Observation Procedure

The right ascension and declination coordinates for the desired object are obtained from an appropriate radio source catalog and entered into the computer. The antenna is slewed by computer to the calculated hour angle and declination position corresponding to these coordinates

Because of the earth's motion, the computer is programmed to continually recalculate the hour angle and declination, and, through the servo loop, keep the antenna tracking the object. The computed hour angle and declination values include correction for atmospheric refraction and building tilt.

Approximately every 15 minutes the computer must be updated for pointing corrections, which are a function of the hour angle position of the antenna. These corrections are necessary because of imperfections in the antenna's bearings, shafts and gears. The pointing correction is determined by observing the limbs of the sun (Fig.3).

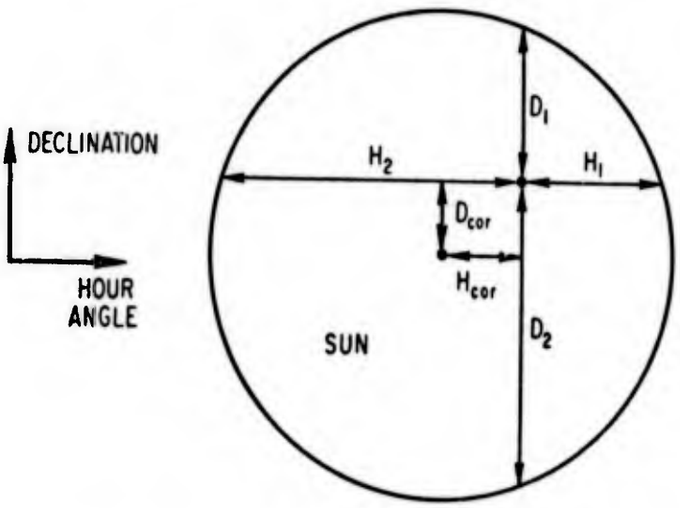

FIGURE 3 POINTING CORRECTIONS

The antenna is commanded to the ephemeris position (which corresponds to the center) of the sun. It is then manually slewed in declination until the received signal

strength indicates the antenna is pointing at a limb. It is then manually slewed back until the opposite limb is reached. The measured angles between the apparent center and the limbs, D1 and D2, yields the declination correction. The hour angle correction is found in the same way.

Approximately every , and always when changing from one object to anothe , a "dipping" measurement is made. This involves observing the "blank sky" at the zenith and at + 30^{0} elevation where the path length through the atmosphere is twice as long as at the zenith. The difference between the two measurements indicates the amount of 3.3-mm radio emission produced by one "unit depth" of atmosphere. This information is used later in correcting for atmospheric attenuation. (Ref. 36).

To cancel the effect of atmospheric emission while observing an object, a dual-beam observing procedure is used. The receiver measures the signal voltage difference between the two antenna beams. The antenna is moved back and forth through 25 minutes of arc (the amount of separation between the two beams) in hour angle so that the object is observed for approximately 92-second intervals, first in one beam and then in the other beam. The beam that is not observing the object is observing only the nearby blank sky. The exact switching interval used is a function of the declination of the object. The interval is determined by how long it takes for the hour angle position of the object to change by 25 minutes of arc. In this way the

beams scan the same arc of hour angle during both halves of a pair of readings (Fig. 4).

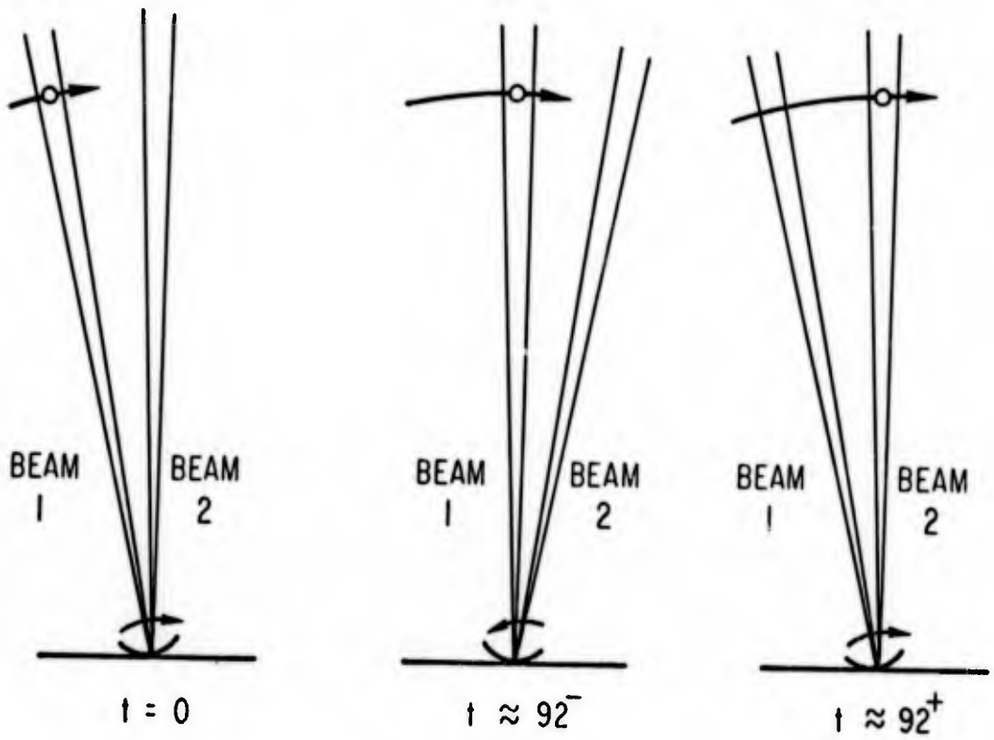

FIGURE 4 DUAL BEAM OBSERVING

The computer, through the analog-to-digital converter samples the receiver output ten times a second. For one observation period this amounts to approximately 920 samples, each of which is the signal difference between the two beams. At the end of the period the computer calculates and prints out the average of the 920 voltage readings and the secant of the zenith angle of the antenna at the end of the period. The next observing period then begins with the antenna moved such that the object is now in the other beam. This procedure is interrupted approximate-

ly every 25 minutes to allow for observation of the hot-load calibration standard. This measurement is used in the reduction of data. The 25 minutes of observation between calibrations is called one cycle. It contains 14 of the approximately 92-second observing periods grouped in seven pairs. Each object was observed for approximately five cycles per day.

The 3.3-mm antenna temperatures of the quasi-stellar objects are $\leq 0.01^{\circ}$ K - i.e., less than the receiver noise. Hence, the object had to be observed, and the signal integrated, for approximately ten hours to achieve signal-to-noise ratios of even a few to one. When a total of 25 cycles was accumulated it was then reduced to yield one flux density value for the object.

Data Reduction

Each cycle of observation is reduced to yield one uncorrected antenna temperature. First the two halves of each of the seven pairs of average voltage readings are subtracted from each other to eliminate the unknown zero point in the antenna temperature scale; the seven results are then averaged. This antenna voltage is converted by the following relation:

$$Ta = \frac{V_a}{V_{cal}} T_{cal} \qquad (2)$$

where V_{cal} is the antenna voltage recorded when observing the hot load calibration standard, and T_{cal} is the effective antenna temperature of the standard found by compar-

ing the voltage measurement of the standard to the voltage measured when observing the sun after it has been corrected for atmospheric effects. The antenna temperature of the sun at 3.3 mm is 5150°K (this temperature was found from the microwave spectrum of the sun and the known characteristics of the antenna).

Since wave propogation in an absorbing medium is accompanied by attenuation, each of the resulting 25 values of T_a' must be corrected for atmospheric attenuation. It has been assumed that the surface of the earth is a flat plane and the atmosphere above it is homogeneous and isothermal.

The observed antenna temperature when the object is in beam 1 is:

$$T'_{a_1} \propto \left[T_o\left(1-e^{-\tau \sec z}\right) + T_a e^{-\tau \sec z}\right] - \left[T_o\left(1-e^{-\tau \sec z}\right)\right] \quad (3)$$

Beam 1 Beam 2

and when the object is in beam 2:

$$T'_{a_1} \propto \left[T_o\left(1-e^{-\tau \sec z}\right)\right] - \left[T_o\left(1-e^{-\tau \sec z}\right) + T_a e^{-\tau \sec z}\right] \quad (3a)$$

Beam 1 Beam 2

where T'_a = observed antenna temperature

T_a = antenna temperature if the observation is made outside the atmosphere

T_o = temperature of the atmosphere

τ = optical depth of a unit thickness of

atmosphere.(atmospheric depth at zenith).

sec z = the multiple of the unit thickness of atmosphere through which T_a was measured

z = angle between the line of observation and the zenith

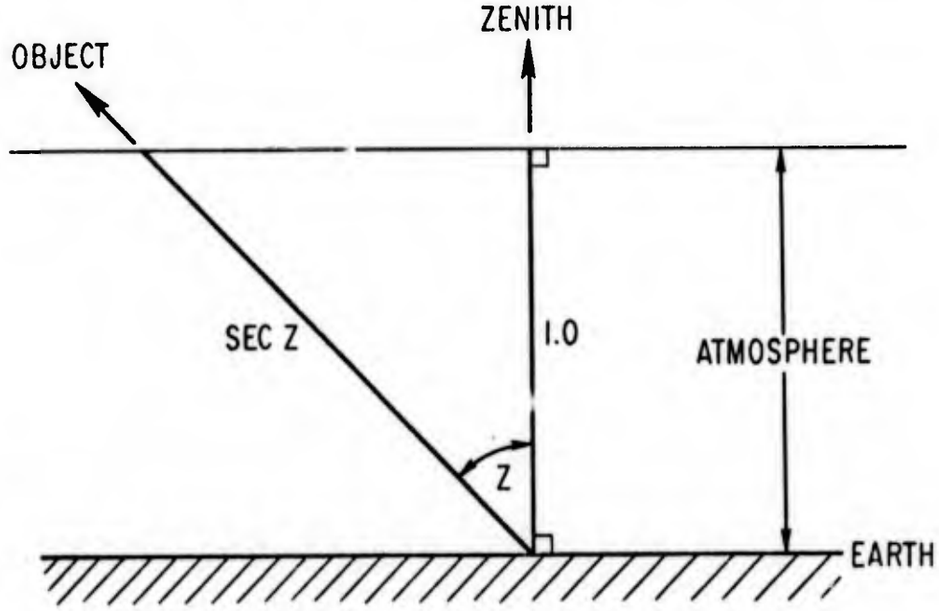

FIGURE 5 SECANT Z

The quantity $e^{-\tau \sec z}$ is the attenuating factor (see appendix A), while $T_o\left(1-e^{-\tau \sec z}\right)$ represents the equivalent antenna temperature of the black body emission from the atmosphere (Appendix B). Because of the dual-beam observing technique the emission term has automatically been accounted for and no correction is necessary here. Equation (3) and (3a) reduce to:

$$T'_{a_1} \propto T_a e^{-\tau \sec z} \qquad (4)$$

$$T'_{a_2} \propto - T_a e^{-\tau \sec z} \qquad (4a)$$

The unknown proportionality constant and hence the unknown

zero point in the scale is eliminated when the pair of readings are subtracted:

$$T'_{a_1} - T'_{a_2} = T'_a = 2T_a e^{-\tau \sec z} \qquad (5)$$

or, equivalently:

$$T_a = \tfrac{1}{2} T'_a e^{\tau \sec z} \qquad (5a)$$

The optical depth, τ, is calculated from the data obtained by the dipping procedure. The difference in atmospheric emission ΔT^{atm} measured at the two zenith angles corresponding to sec z = 1 and sec z = 2 is:

$$\Delta T_{atm} = T_o\left[\left(1-e^{-\tau}\right) - \left(1-e^{-2\tau}\right)\right] = T_o\left(e^{-2\tau}-e^{-\tau}\right) \qquad (6)$$

If T_o is known, then an approximate value of τ can be obtained. However, in equation (6) T_o is considered as constant, which is not true in the real atmosphere. An empirical relation between τ and the differential emission measured by the dipping procedure has been derived at a wavelength of 3.3 mm (Ref.8) and it is used to find the value of τ.

The 25 corrected antenna temperatures, T_a are averaged and the results converted to units of flux. One flux unit equals 10^{-26} watt/Meter^2 Hz. Antenna temperature is directly proportional to flux density:

$$S = \frac{2kTa}{A} \qquad (7)$$

where S = flux density in watt/M^2/Hz

T_a = antenna temperature in degrees Kelvin

k = Boltzman constant

A = effective aperture of the antenna

The effective aperture of the antenna is found from the gain measurement with:

$$G = \frac{4\pi A}{\lambda^2} \tag{8}$$

where G = measured gain at 3.3 mm

λ = wavelength

The final result is one measurement of the flux density emitted by the object during the period of time the 25 cycles of observation were made.

III. Theory

In the model it is assumed that an event is initiated when, at some small region or point on or in a QSS or radio galaxy, a compact cloud of relativistic electrons is produced by an unknown process. The resulting radio source then consists of a homogeneous, adiabatically expanding sphere of these electrons emitting synchrotron radiation. The magnetic field is assumed randomly oriented throughout the source and is conserved. The relativistic electrons obey Fermi-Dirac statistics and are assumed to have an isotropic energy distribution of the form:

$$N(E)dE \propto K(r)E^{-\gamma}dE \tag{9}$$

where $N(E)dE$ = number density of electrons with energy between E and E + dE

$K(r)$ = number density of electrons

γ = constant

r = total radius of the source

It will be shown (eq. 21b) that the electrons lose energy as r^{-1} (Ref.37:244) because of the adiabatic expansion. The total number of electrons is assumed conserved.

The amount of self-absorption of radiation accuring within a source is proportional to the value of the self-absorption coefficient. It will be shown (eq. 14 and 21) that the self absorption coefficients dependence on radius of the source is:

$$\chi(r) \propto r^{-2(\gamma+2)} \tag{10}$$

where $\chi(r)$ = self-absorption coefficient

r = total radius of the source

Initially, (when r is small), the self-absorption coefficient is very large and the source is opaque to its own radiation. It will also be shown (eq.22) that in this phase of the evolution of a source the flux density emitted at a frequency ν will increase as r^3. As the absorption coefficient decreases due to the expansion, the source will become partially transparent at a given frequency and the observed flux density will reach a maximum. It will then be shown (eq. 23) that the flux density decays as $r^{-2\gamma}$ as the source continues to expand. Since the absorption coefficient varies as $r^{-2(\gamma+2)}\ \nu^{-(\gamma+4)/2}$, the source will become transparent at successively lower frequencies as r increases. Because of the energy density decrease in the expansion, the amplitude of the flux density maximum will be less at later times as the maximum is observed at lower frequencies. At wavelengths longer than 20 or 30 cm the change in flux density becomes negligible against the background radiation.

Two or more events may be evolving simultaneously in one object. The radiation from each event plus any background radiation from the object combine to form the total spectrum. The events may be in different stages of evolution and may be spatially separated. Because the theory deals only with an isolated, non-interacting outburst, an attempt is made (Section IV) to resolve the varying com-

ponent of the total spectrum due to the outburst under investigation from the remainder of the emitted radiation.

Predicted Behavior

A detailed calculation by Le Roux (Ref.23:79-81) has shown that, for a source of synchrotron radiation in a uniform sphere of diameter l, in a magnetic field of strength B, the solution of the equation of transfer:

$$\frac{dI}{dl} = -\chi I + J \qquad (11)$$

where I = intensity

χ = absorption coefficient

J = mean emission per unit volume

in terms of flux density, is:

$$S(\nu) = l^2 \frac{J(\nu)}{\chi(\nu)} \left(1-e^{-\tau(\nu)}\right) \qquad (12)$$

where $S(\nu)$ = flux density at frequency ν

τ = optical thickness $\equiv \int \chi(\nu) dl = \chi(\nu) l$

The volume emissivity and absorption coefficient for synchrotron radiation as derived by Le Roux are:

$$J(\nu) = \frac{\mu K e^2 C}{8\pi R^2} \left(\frac{eB}{2\pi M_o}\right)^{\frac{\gamma+1}{2}} F(\gamma)\, \nu^{\frac{1-\gamma}{2}} \qquad (13)$$

Note that Le Roux has incorporated the R^{-2} dependence of the radiation in J rather than in S as is usually done.

and

$$\chi(\nu) = \frac{\mu K e^2 c}{16\pi m_o} \left(\frac{eB}{2\pi m_o}\right)^{\frac{\gamma+2}{2}} (\gamma+2) G(\gamma) \nu^{-\frac{\gamma+4}{2}} \qquad (14)$$

where μ = permeability

K = electron density

e = charge of electron

c = speed of light

R = distance of the source from observer

B = magnetic field strength

m_o = rest mass of an electron

γ = index of the electron energy distribution

ν = frequency

$G(\gamma)$ and $F(\gamma)$ are numerical factors close to unity which are only weakly dependent on γ.

The angular diameter of the source, θ, is proportional to the linear extent of the source, l.

At any instant of time there will be one particular frequency at which the flux density has just reached its maximum value. At this instant of time and this frequency $\tau \approx 1$. For frequencies $\nu \ll \nu_m$, the frequency of maximum flux density, the source is still optically thick and $\tau \gg 1$. In this case the factor $\left(1 - e^{-\tau}\right)$ is approximately equal to one and from equation (12):

$$S(\nu) \approx l^2 \frac{J(\nu)}{\chi(\nu)} \approx K_1 B^{-\frac{1}{2}} \theta^2 \nu^{5/2} \qquad (15)$$

where

$$K_1 = \left(\frac{8\pi m_o}{e}^3\right)^{\frac{1}{2}}$$

The frequency dependence of the spectral curve takes the form:

$$S \propto \nu^{5/2} \qquad \nu \ll \nu_m \tag{16}$$

For frequencies $\nu \gg \nu_m$ the source is optically thin ($\tau \ll 1$) and here the factor $\left(1 - e^{-\tau}\right)$ is approximately equal to τ; from equation (12):

$$S(\nu) \approx l^3 J(\nu) = KK_2 B^{\frac{\gamma+1}{2}} \theta^3 \nu^{\frac{1-\gamma}{2}} \tag{17}$$

where

$$K_2 = \frac{\mu Re^2 C}{8\pi} \left(\frac{e}{2\pi m_o}\right)^{\frac{\gamma+1}{2}}$$

The frequency dependence of the spectral curve now takes the form:

$$S \propto \nu^{\frac{1-\gamma}{2}} \qquad \nu \gg \nu_m \tag{18}$$

At the frequency ν_m the optical depth is approximately unity, hence:

$$1 \approx l\chi(\nu_m) \tag{19}$$

Dividing equation (17) by (19) yields a relation between the frequency of the maximum flux density and any higher frequency:

$$\frac{S(\nu_t)}{1} \approx \frac{l^3 J(\nu_t)}{l\chi(\nu_m)} = \frac{\frac{\mu e^2 C}{8\pi}\left(\frac{e}{2\pi m_o}\right)^{\frac{\gamma+1}{2}} KRB^{\frac{\gamma+1}{2}} \theta^3 \nu_t^{\frac{1-\gamma}{2}}}{\frac{\mu e^2 C}{16\pi m_o}\left(\frac{e}{2\pi m_o}\right)^{\frac{\gamma+2}{2}} KlB^{\frac{\gamma+2}{2}} \nu_m^{-\frac{\gamma+4}{2}}} \tag{20a}$$

$$S(\nu_t) = \left(\frac{8\pi m_o^3}{e}\right)^{1/2} B^{-1/2}\ \theta^2\ \nu_t^{\frac{1-\gamma}{2}}\ \nu_m^{\frac{\gamma+4}{2}} \qquad (20b)$$

$$\nu_m = \left[\left(\frac{e}{8\pi m_o^3}\right) B\ \theta^{-4}\ S(\nu_t)^2\ \nu_t^{\gamma-1}\right]^{\frac{1}{\gamma+4}} \qquad (20c)$$

where ν_t = a frequency at which the source is transparent (note $\nu_t > \nu_m$).

The parameters B,E,K, and θ, change as the adiabatic expansion proceeds from the time T_o. (The subscript "o" denotes values at a specified instant) It is assumed that the general structure of the magnetic field remains unchanged during the expansion. It is assumed the magnetic flux is conserved and the field strength varies as:

$$B = B_o\left(\frac{r}{r_o}\right)^{-2} \qquad (21a)$$

where r = radius of the expanding sphere.

The relativistic electron gas cools adiabatically and from the adiabatic invariance of

$$\frac{P_\perp^2}{B} = \text{constant}$$

where $P_\perp$ = the component of the electrons momentum perpendicular to B

the energy of an individual electron perpendicular to B varies as:

$$E = E_o\left(\frac{r}{r_o}\right)^{-1} \qquad (21b)$$

It has been shown (Ref.9 and 29) that even if the magnetic field is unusually strong, e.g., 10^{-3} gauss, the effect of energy loss by synchrotron radiation on the radio spectrum or the electron energy distribution index will not manifest itself at frequencies below 100 GHz until at least three years after the initiation of the event. Observations indicate that subsequent outbursts have usually occured within that interval with the result that analysis of the original outburst, which is decaying rapidly, is impossible. In any case, it seems likely that by the time this stage is reached the effect of synchrotron radiation losses and the expansion of the original outburst will cause the intensity of emitted radiation to be very low, and the outburst will have become too weak to observe. Therefore, in the time interval of interest here, all electrons will appear to lose energy in the same ratio. Hence, their energy spectrum will remain constant. If when $r = r_o$, the energy spectrum was of the form $N(E)dE = K_o E_o^{-\gamma} dE$ then at later times, γ = constant, while K, from

$$r^3 K \int E^{-\gamma} dE = r_o^3 K_o \int E_o^{-\gamma} dE$$ (conservation of electrons) will vary as:

$$K = K_o \left(\frac{r}{r_o}\right)^{-(\gamma+2)} \qquad (21c)$$

The angular diameter varies as:

$$\theta = \theta_o \frac{r}{r_o} \qquad (21d)$$

From relation (15) and (21) the flux density as a function of radius for the region where $\tau \gg 1$ is:

$$S = S_o \left(\frac{r}{r_o}\right)^3 \tag{22}$$

Similarly, from relations (17) and (21), the functional dependence of the flux density on radius for the region where $\tau \ll 1$ is:

$$S = S_o \left(\frac{r}{r_o}\right)^{-2\gamma} \tag{23}$$

The dependence of ν_m on radius is obtained from equations (20c), (21) and (23):

$$\nu_m = \nu_{m_o} \left(\frac{r}{r_o}\right)^{\frac{-4\gamma+6}{\gamma+4}} \tag{24}$$

The variation of the maximum flux density with the radius follows from equations (16), (22) and (24) or equations (18), (23) and (24):

$$S_m = S_{m_o} \left(\frac{r}{r_o}\right)^{-\frac{7\gamma+3}{\gamma+4}} \tag{25}$$

From (24) and (25) the relationship between the maximum flux density and the frequency at which it occurs is:

$$S_m = S_{m_o} \left(\frac{\nu_{m_o}}{\nu_m}\right)^{\frac{-7\gamma+3}{4\gamma+6}} \tag{26}$$

or the equivalent expression

$$S_m = S_{m_o} \left(\frac{\lambda_m}{\lambda_{m_o}}\right)^{\frac{-7\gamma+3}{4\gamma+6}} \tag{27}$$

where λ = wavelength

Time Dependence

The observed variations of the sources are recorded as a function of time, not radius. Therefore, in order to obtain an expression for the flux density at any frequency as a function of time, it is necessary to specify either the time dependence of the expansion velocity, or the time dependence of the radius of the source. With the expansion velocity assumed constant:

$$r = r_o \frac{t}{t_o} \tag{28}$$

where t = the age of the source of radius r

It has been suggested (Ref.3) that an acceleration parameter β, be introduced such that

$$r = r_o \left(\frac{t}{t_o}\right)^{\beta} \tag{29}$$

where β = 1 if the velocity is constant

$\beta > 1$ if the expansion is accelerating

$\beta < 1$ if the expansion is decellerating

The expansion may be slowed down by the intergalactic medium or the relativistic particles may still be accelerating, perhaps due to their continuing generation. In an attempt to remain as general as possible, relation (29) is used here. Therefore, from (22) and (29) the time dependence of the flux density when $\tau \gg 1$ is:

$$S = S_o \left(\frac{t}{t_o}\right)^{3\beta} \tag{30}$$

When $\tau \ll 1$, from (23) and (29) it is:

$$S = S_o \left(\frac{t}{t_o}\right)^{-2\gamma\beta} \tag{31}$$

The change in the frequency of maximum flux density with time follows from equations (24) and (29):

$$\nu_m = \nu_{m_o} \left(\frac{tm}{tm_o}\right)^{-\beta\left(\frac{4\gamma+6}{\gamma+4}\right)} \tag{32}$$

or, equivalently,

$$tm = tm_o \left(\frac{\lambda_m}{\lambda_{m_o}}\right)^{\left(\frac{\gamma+4}{(4\gamma+6)\beta}\right)} \tag{33}$$

The time variable in the above relations refers to the age of the source and can be expressed as $(T - T_o)$ such that:

$$t = (T - T_o) \tag{34}$$

where t = age of event

T = local time of observation

T_o = local time of the initiation of the event.

Summary

The equations which describe the behavior of the flux density variations from an expanding source of synchrotron radiation are:

$$S \propto \nu^{5/2} \quad \text{valid for} \quad \nu \ll \nu_m \tag{35}$$

$$S \propto \nu^{\frac{1-\gamma}{2}} \quad \text{valid for} \quad \nu \gg \nu_m \tag{36}$$

$$S_m \propto \lambda_m^{-\left(\frac{7\gamma+3}{4\gamma+6}\right)} \text{ valid for } \nu = \nu_m \tag{37}$$

$$S \propto (T - T_o)^{3\beta} \text{ valid for } \nu \ll \nu_m \tag{38}$$

$$S \propto (T - T_o)^{-2\gamma\beta} \text{ valid for } \nu \gg \nu_m \tag{39}$$

$$(T_m - T_o) \propto \lambda_m^{\frac{\gamma+4}{(4\gamma+6)\beta}} \tag{40}$$

These equations are used in Section IV to compare the expanding source model with the observations.

IV. Analysis and Discussion

The data used in this analysis, at each wavelength, is presented, for each object, as a series of flux density versus time plots, all sharing the same time scale. In this way the increase of flux density due to an outburst can be seen to occur first at the highest frequency observed and then, as the radio source evolves, at progressively lower frequencies with increasing time. The data at each wavelength is the result of a superposition of at least two components; the background or quiescent component, which may be varying slowly, and the rapidly varying component, due to an outburst in the object. Frequently, two or more events are evolving simultaneously, with the result that the observed flux density is a composite of the quiescent and all the rapidly varying components. Resolution of the data into the individual components was accomplished by extrapolating the trends of the variations observed and subtracting the contribution of all components not being analyzed from the measured value of the flux density. This manipulation, while admittedly only an estimate, is the only technique available.

The corrected data for each event is used to test the predictions developed in the preceeding section. First relation (38) is rewritten as:

$$T_o = \frac{\left(\frac{S_1}{S_2}\right)^{\frac{1}{3\beta}} (T_2 - T_1)}{\left(\frac{S_1}{S_2}\right)^{\frac{1}{3\beta}} - 1} \qquad (41)$$

where T_o = time the event was initiated, years

S_1 = flux density at time, T_1, flux units

S_2 = flux density at time, T_2, flux units

β = acceleration parameter

Equation (41) is valid for $\tau \gg 1$, i.e., at any given wavelength, the interval of time when the flux density is increasing. A program to repeatedly solve equation (41) for adjacent pairs of S_1 and S_2 was written in Fortran IV for a Control Data Corporation (CDC) 6000 series computer . For each solution β was varied as a parameter in steps of 0.1 from a value of 0.5 to 1.5. This program was run, using data at each wavelength where the event was adequately observed. The equation plus the constraint that it yields the same result at every wavelength allows for the simultaneous solution of T_o and β. The results of the analysis are displayed graphically as T_o vs λ for each β.

Next, relation (39) is put in the form:

$$\gamma = \frac{\text{Log}\left(\frac{S_1}{S_2}\right)}{2\beta \text{Log}\left(\frac{T_2 - T_o}{T_1 - T_o}\right)} \qquad (42)$$

where γ = electron energy distribution index

where S_1 = flux density at time T_1, flux units

S_2 = flux density at time T_2, flux units

β = acceleration parameter

This relation is valid only for $\tau \ll 1$, i.e., at any given wavelength, the interval of time when the flux density is decreasing. With the values of T_o and β found above, equation (42) was solved repeatedly, by computer, for γ from adjacent pairs of S_1 and S_2 at each wavelength where the event's decay was adequately observed. The value of γ most consistent with the solution at every wavelength was taken to be the γ for that event.

With the values of T_o, β, and γ determined for each event, the observed time of maximum flux density, T_m, at each wavelength is used to test the validity of the model by plotting $(T_m - T_o)$ vs λ on a log log graph and comparing its slope to $(\gamma+4)/(4\gamma+6)\beta$ which is the slope predicted by equation (40). Similarly, the observed value of the maximum flux density, S_m, reached at each wavelength is plotted versus λ on a full log graph and the slope compared to a value of $-(7\gamma+3)/(4\gamma+6)$ which is the slope predicted by equation (37). As an additional test of the model, a full log plot of flux density versus frequency is made for a few points in time during the evolution of each event. The slope of the spectrum is compared to the slope expected if the model is accurate. Equations (35)and(36) predict a slope of 2.5 for the region of the spectrum where the flux density is increasing

and a slope of $(1-\gamma)/2$ for the region of decreasing flux density.

In the model the assumption was made that the magnetic field strength $B \leq 10^{-3}$ gauss. An estimate of the upper limit of the magnetic field strength is obtained from equation (20c). Solving for B and evaluating the constant yields:

$$B \approx 10^{-8} \theta^4 \, S^{-2}(\nu_t) \, \nu_t^{1-\gamma} \, \nu_m^{\gamma+4} \tag{43}$$

where B = magnetic field strength, gauss

θ = angular diameter, sec of arc

$S(\nu_t)$ = flux density at ν_t, flux units

ν_t = frequency, MHz ($\nu_t > \nu_m$)

ν_m = frequency of maximum flux density, MHz

The value for the upper limit of θ is obtained by assuming an expansion velocity equal to the speed of light. Therefore:

$$\theta < 2.06 \times 10^5 \, \frac{\text{lmax}}{R} \tag{44}$$

where θ = angular diameter, arc sec

lmax = maximum linear extent, parsec

R = distance to the source, parsec

with

$$\text{lmax} = Ct_m \tag{45}$$

where C = velocity of light, parsec/yr

t_m = age of the source corresponding to ν_m, $(T_m - T_o)$, yr.

The values of R, the distance to the source is determined from the cosmological interpretation of the object's red

shift by:

$$R = \frac{CZ}{H_o} \tag{46}$$

where R = distance to the source, Mpc

$Z = \frac{\Delta\lambda}{\lambda_o}$ = red shift

C = velocity of light, m sec^{-1}

H_o = Hubble constant, m sec^{-1} Mpc^{-1}

$\Delta\lambda$ = wavelength difference or shift in wavelength

λ_o = unshifted wavelength

The exact value for Hubble's constant is uncertain, but it lies within $1.0 \pm 0.5 \times 10^5$ m sec^{-1} Mpc^{-1}.

3C84

3C84, also called NGC 1275, is a Seyfert galaxy with a red-shift equal to 0.018 (Ref.30:843). It is, from equation (46), approximately 54 Mpc distant. The radio energy received from this object, therefore, originated about 173 million years ago. In Fig. 6 is presented the flux density received from 3C84 from 1965 to late 1969 at wavelengths from 3.3 mm to 6 cm. The data suggests the presence of 3 separate events during this interval, with event I being adequately observed first at 3.3 mm in 1966.4 and continuing until 1967.4 at 6 cm. Event II is first noted in 1967.2 at 9.55 mm and is observed until 1969.4 at 6 cm. Event III first appears in 1967.5 at 9.5 mm and is last seen accurately in 1969.1 at 2 cm. The suggested curve through the 9.55-mm data clearly shows the 3 increases in the flux density. The shape of the 1967.0 rise at 1.55 cm shows a broadening effect compared to the shape at 9.55 mm. This trend continues until, at 2 cm, the effect is to lengthen and confuse the increase at 2 cm due to event I to the point where it completely obscures the increase due to event II and III. Because of the scatter in the 2.8-cm and 4.5-cm data no reliable trends could be found. The quiescent component at 3.3 mm is about 10 flux units and is fairly constant, while at 9.55 mm, 1.55 mm, 2 cm, and 6 cm it shows a slow steady increase with mean values of approximately 27, 31, 29, and 16 flux units respectively.

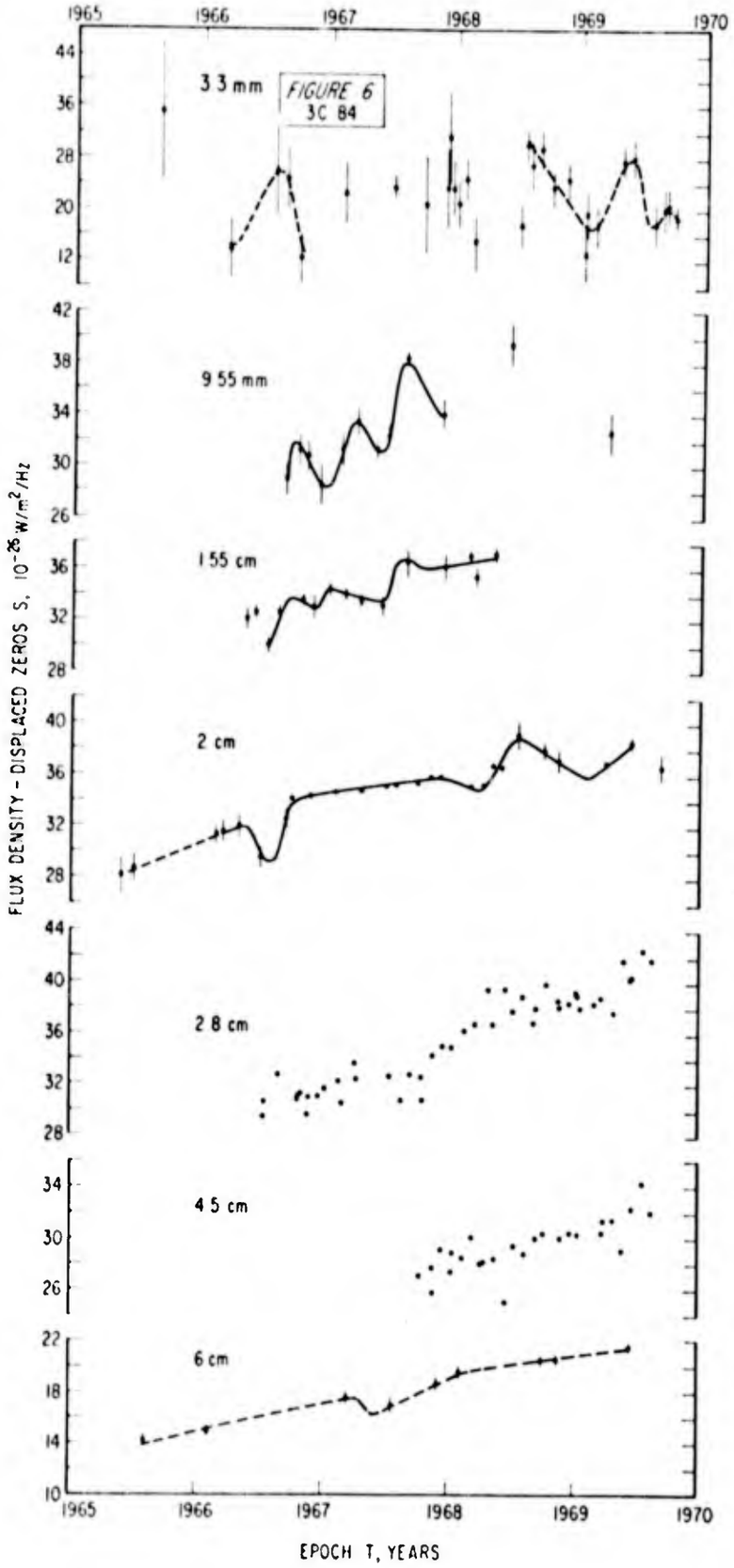
1965
1966
1967
1968
1969
1970
3 3 mm
FIGURE 6
3C 84
9 55 mm
1 55 cm
2 cm
2 8 cm
4 5 cm
6 cm
FLUX DENSITY - DISPLACED ZEROS S, 10^{-26} W/m^2/Hz
EPOCH T, YEARS

Event I. The flux density increases at 3.3 mm, 9.55 mm, 1.55 cm and 2 cm are used in equation (41) with the results indicated in Fig. 7. The error bars for all the points are of the same order of magnitude as those shown for $\beta = 0.5$, but are left off for clarity. The results of this computation suggest values of T_o and β of 1966.40 and 1.0 respectively.

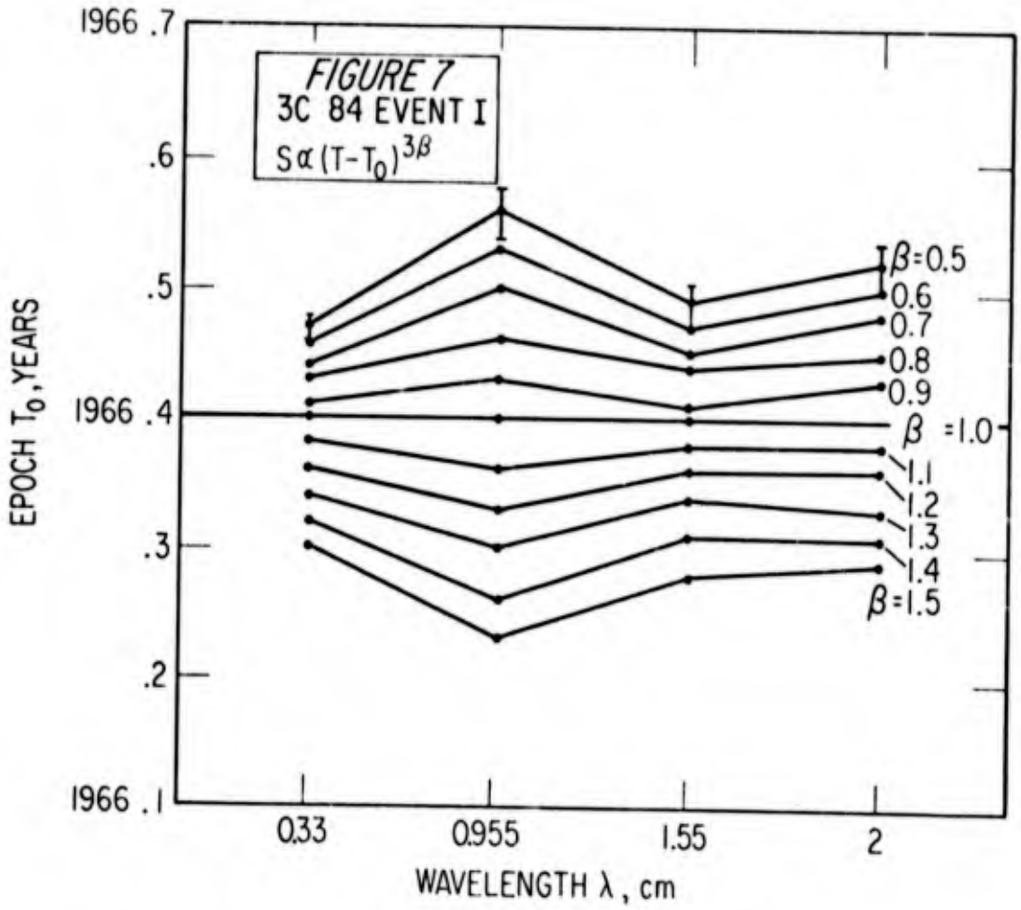

With these values to T_o and β equation (42) is evaluated for the flux density decreases at 3.3 mm, 9.55 mm and 1.5 cm. The value of γ which best fits the results at each wavelength is $\gamma = 1.0 \pm 0.1$. From Fig. 6 the

epochs of the maximum flux density, T_m, at the wavelengths 3.3 mm, 9.55 mm, 1.55 cm, 2 cm and 6 cm are 1966.6 ± 0.05, 1966.74 ± 0.05, 1966.75 ± 0.05, 1966.78 ± 0.05 and 1967.2 ± 0.1, respectively. The age of these maxima, $(T_m - T_o)$, are plotted against wavelengths on Fig. 8. The slope of t_m vs λ as predicted by equation (40) with $\gamma = 1.0 \pm 0.1$ and $\beta = 1.0$, is 0.5 ± 0.01. The data is consistent with the derived values of γ and β and equation (40).

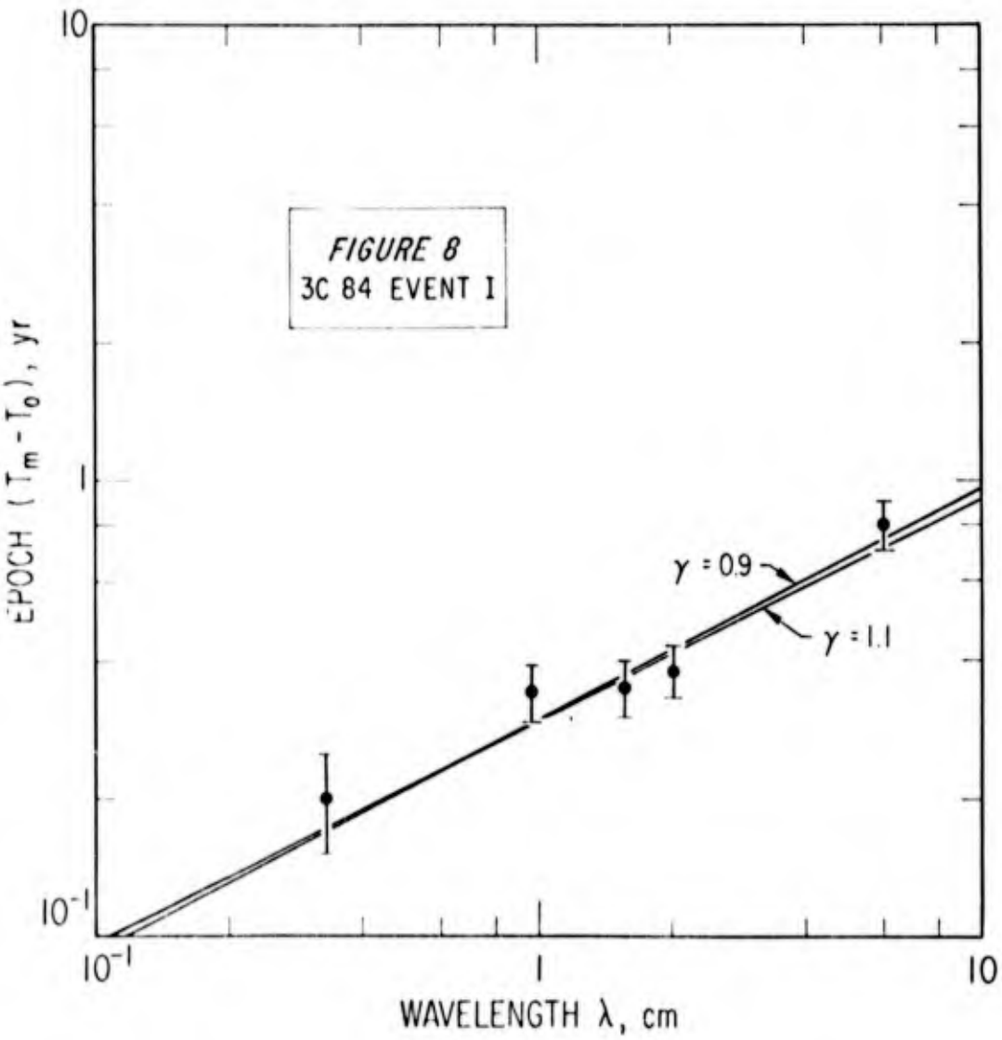

The value of the maximum flux density reached at each of these wavelengths is displayed in Fig. 9 with the range of slope predicted by equation (37) superimposed on this data. With $\gamma = 1.0 \pm 0.1$, the exponent (the slope on a log-log graph) in equation (37) is equal to -1.0 ± 0.03. Again, the data is consistent with the prediction.

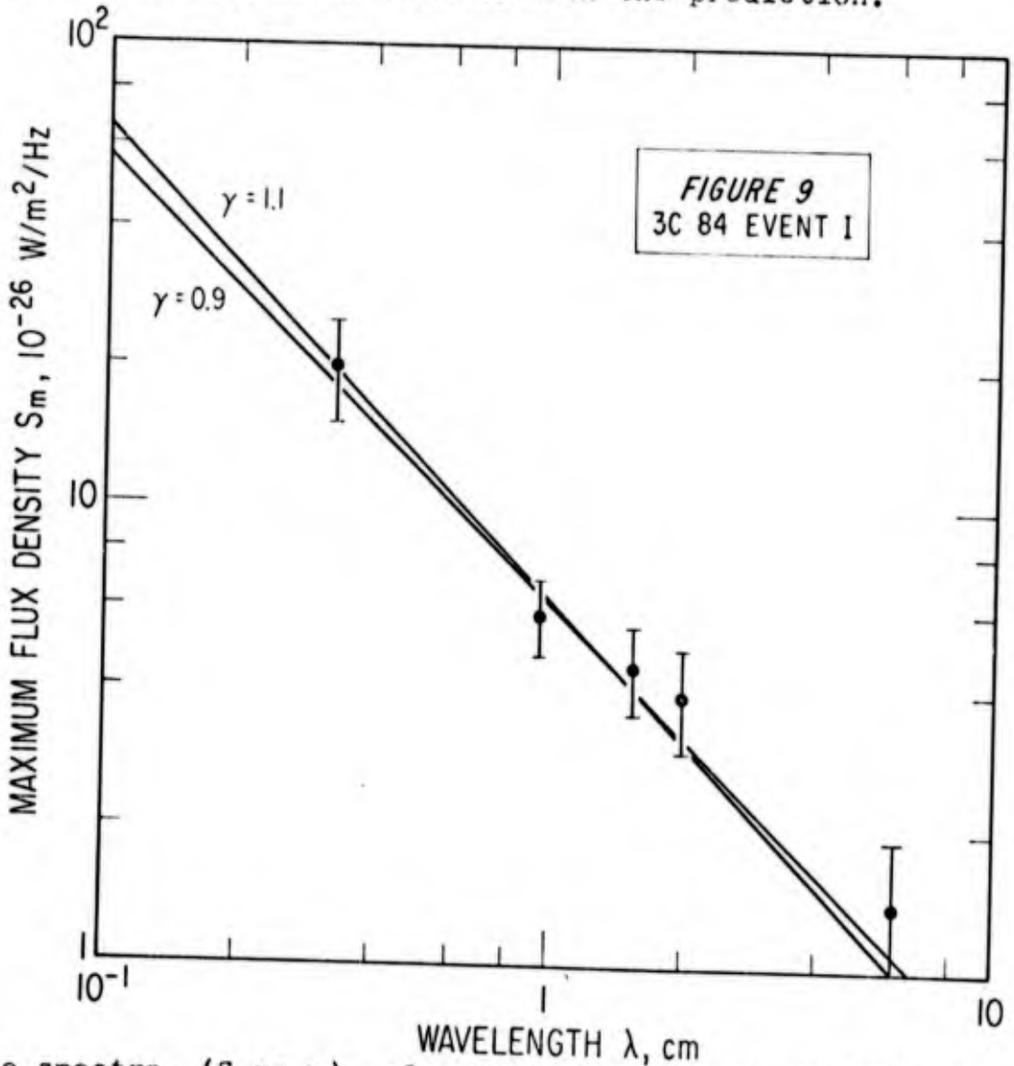

The spectra, (S vs ν), of event I for the epochs 1966.5, 1966.7, 1966.9 are plotted in Fig. 10. Equation (35) predicts a slope of 0.0 ± 0.05 for the points where S is decreasing. These slopes are shown superimposed on the data for each epoch in Fig. 10 and are consistent

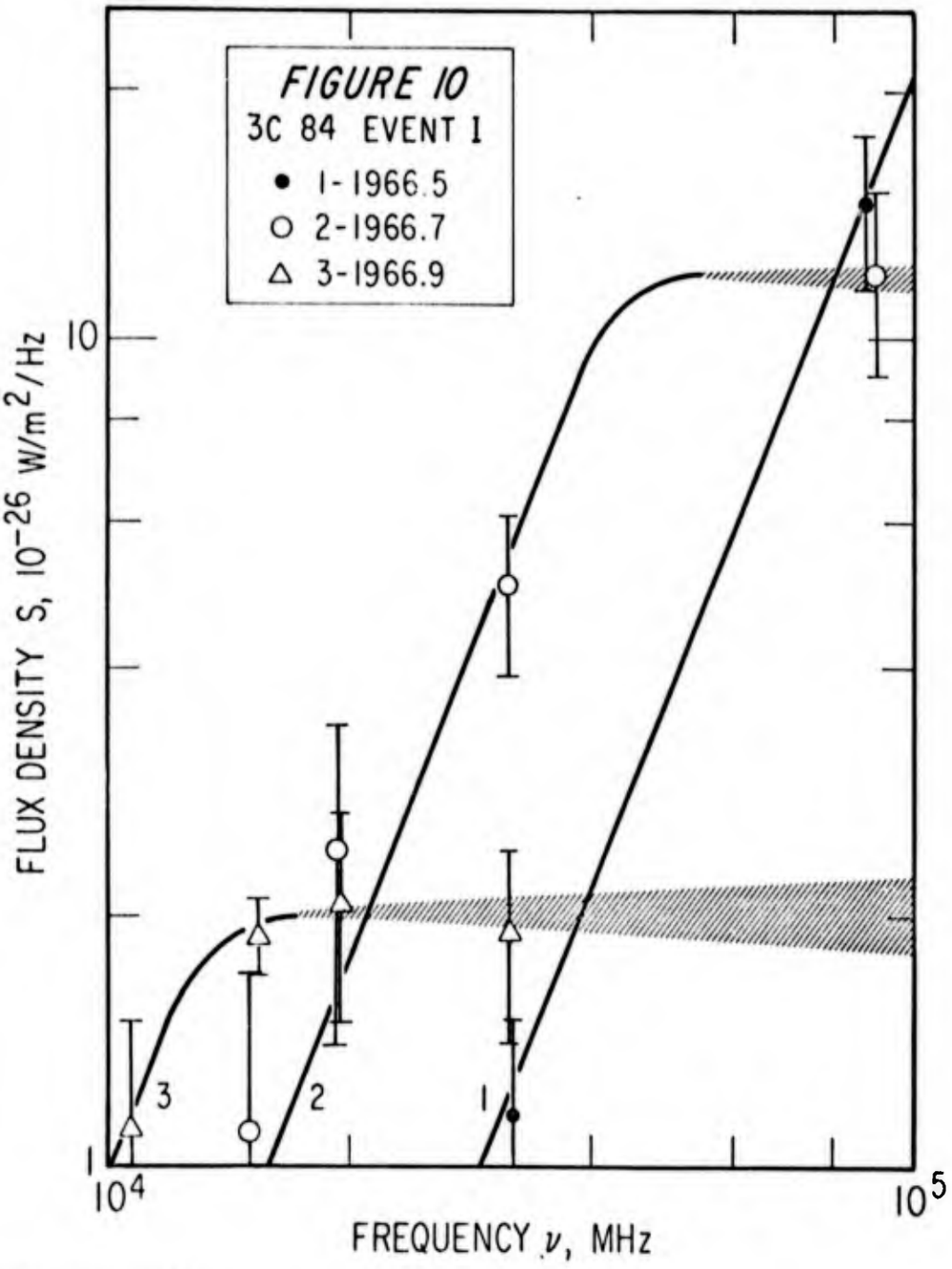

with the data.

The maximum linear extent of the source at the time when the flux density reached a maximum at 1.55 cm (1966.75) computed from equation (45), was 4.2 light months. This corresponds to an angular size, from equation (44), of 0.0004 arc sec. Evaluating equation (43) with $\nu_t=9.08\times10^4$

MHz (3.3 mm) the value of the magnetic field strength was equal to or less than 2×10^{-5} gauss.

Event II. Equation (41) was evaluated with data from the flux density increases at 3.3 mm, 9.5 mm, 1.55 cm, and 6 cm and the results are shown in Fig. 11.

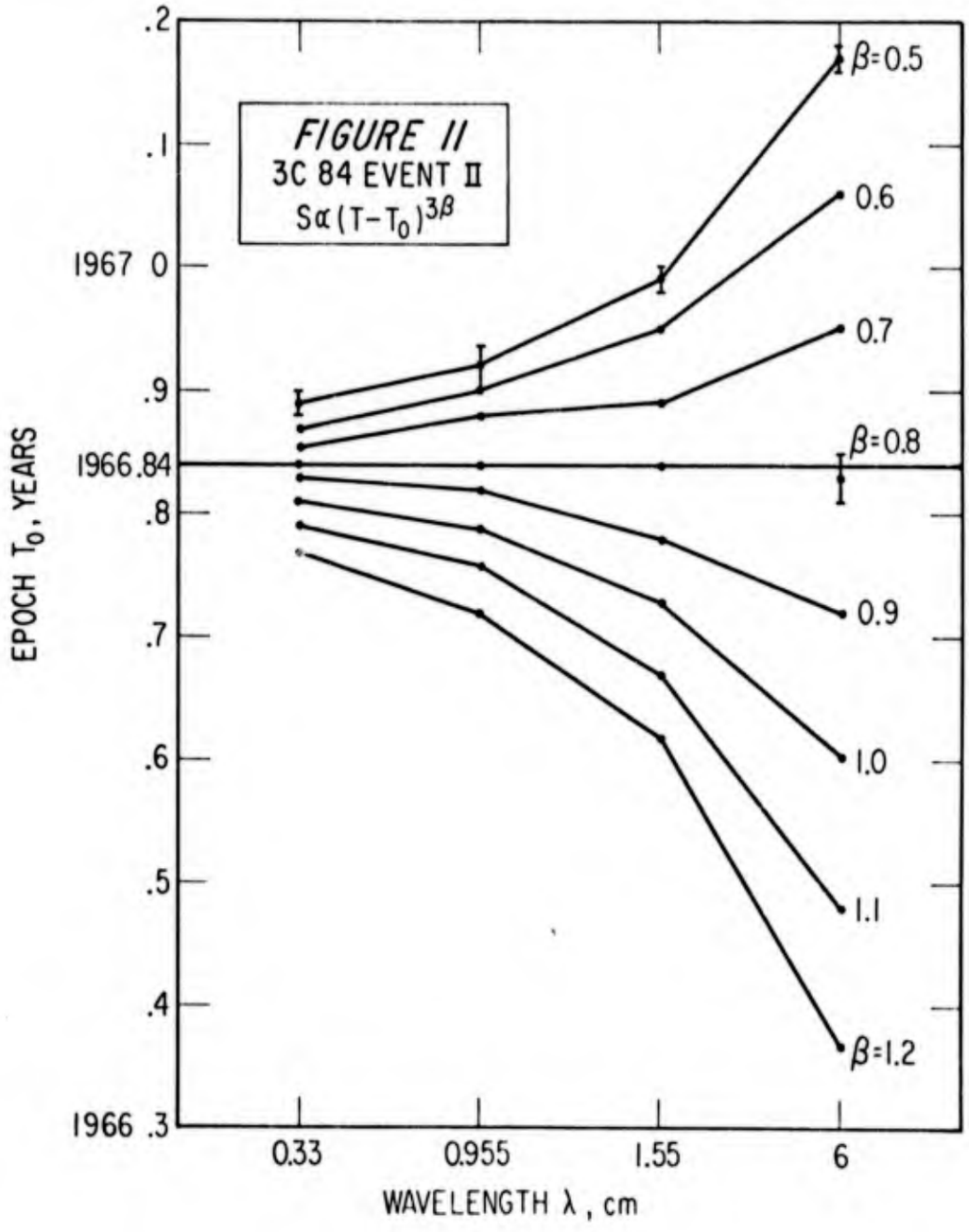

Again, the error bars have been left off most of the points for the sake of clarity. T_o is found to be equal to 1966. 84 ± 0.04 with β equal to 0.8. Using these values in equation (42) and the flux density decreases 9.55 mm, 1.55 cm and 2 cm, γ is found to be equal to 1.5 ± 0.1.

The epochs of the maximum, from Fig. 6 are; 3.3 mm- 1967.0 ± 0.1 (interpolated), 9.55 mm - 1967.21 ± 0.04, 1.55 cm - 1967.08 ± 0.04, 6 cm - 1967.24 ± 0.05. The ages of these maxima versus wavelength are shown in Fig. 12 together with the slope predicted by equation (40) for the values of γ and β found above.

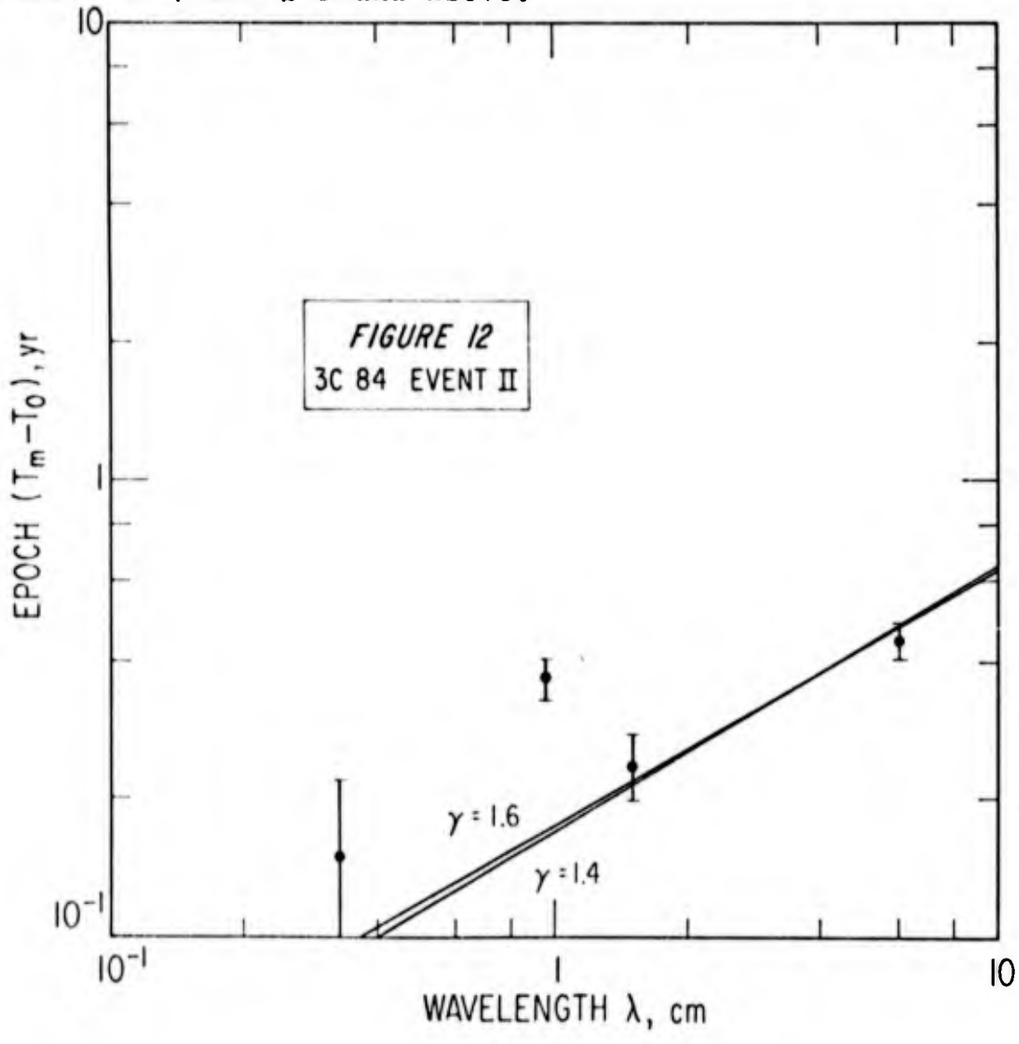

FIGURE 12
3C 84 EVENT II

This slope (0.573 ± 0.00[illegible]) can not be positioned to include the point at 9.55 mm. The values of these maxima versus wavelength are shown in Fig. 13 together with the slope predicted by equation (37), which for $\gamma = 1.5 \pm 0.1$ is $- 1.125 \pm 0.02$.

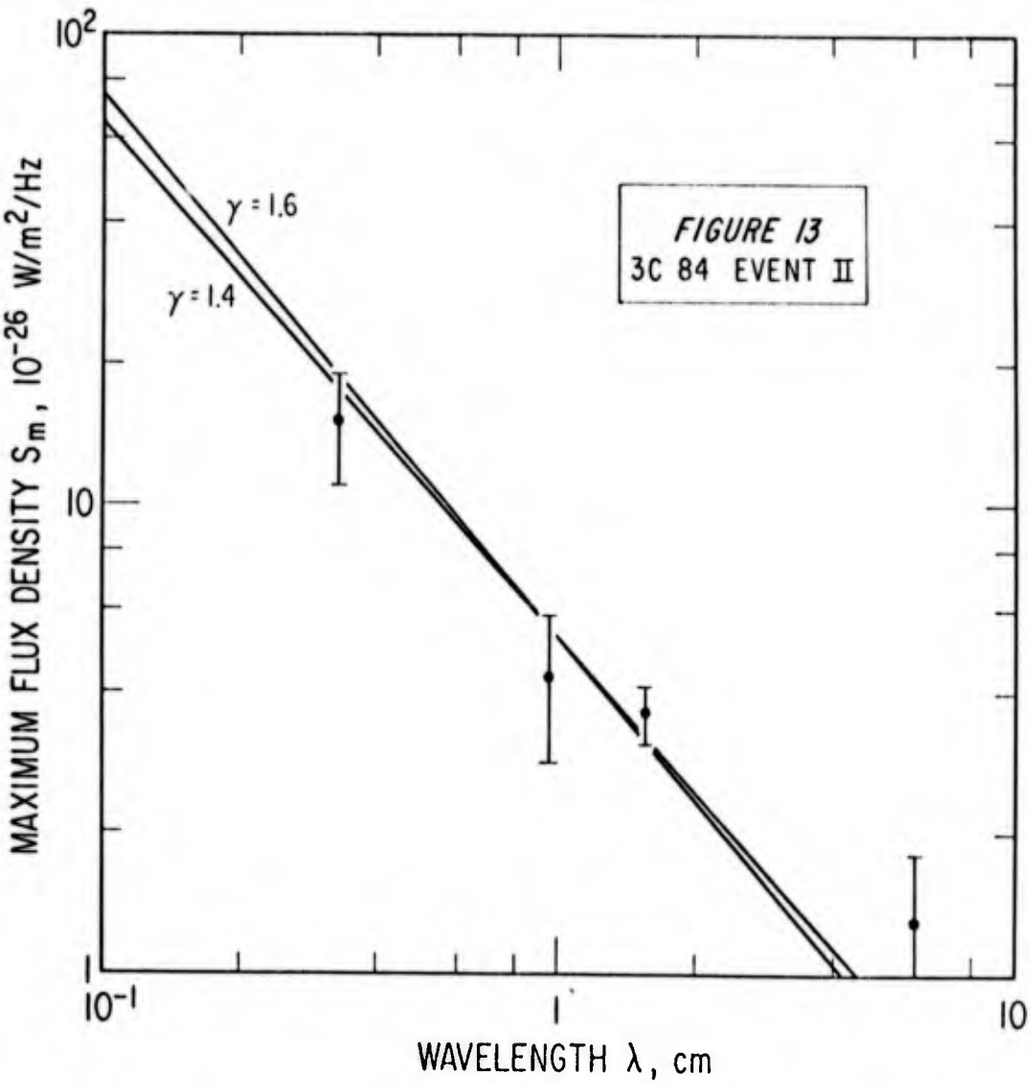

The spectra of event II for the epochs 1967.0, 1967.2, and 1967.4 are shown in Fig. 14 together with the slopes 2.5 and $- 0.25 \pm 0.05$ predicted by equations (35) and (36).

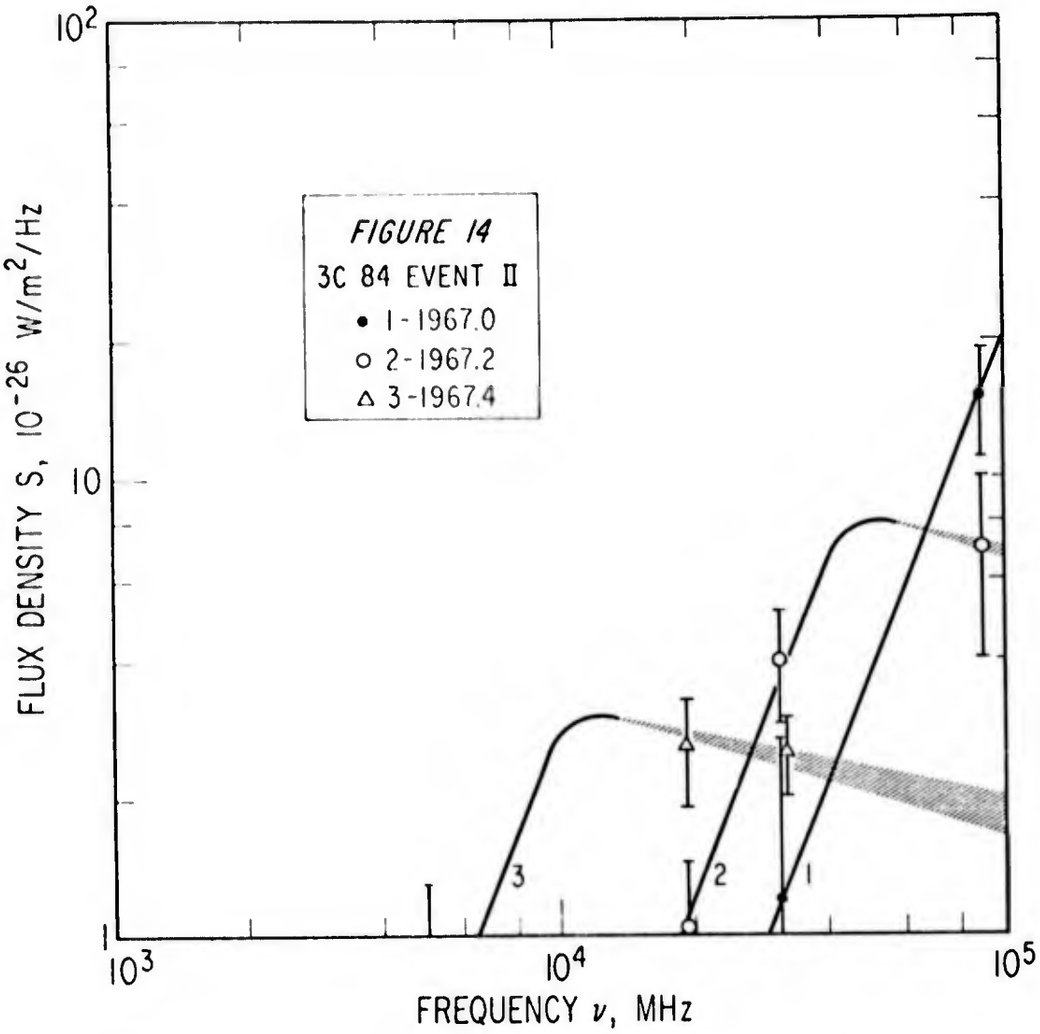

The maximum linear extent of the source when the flux density reached a maximum at 1.55 cm was 2.9 light months. This corresponds to an angular size of 0.0003 arc sec. With $\nu_t = 9.08 \times 10^4$ MHz, equation (43) yields a maximum magnetic field strength of 3.6×10^{-4} gauss.

Event III. Event III was observed completely only at 9.55 mm and 1.55 cm and partially at 2 cm. Fig. 15 shows the results of analysis of relation (41), which yielded $T_o = 1967.37 \pm 0.05$ and $\beta = 1.0$.

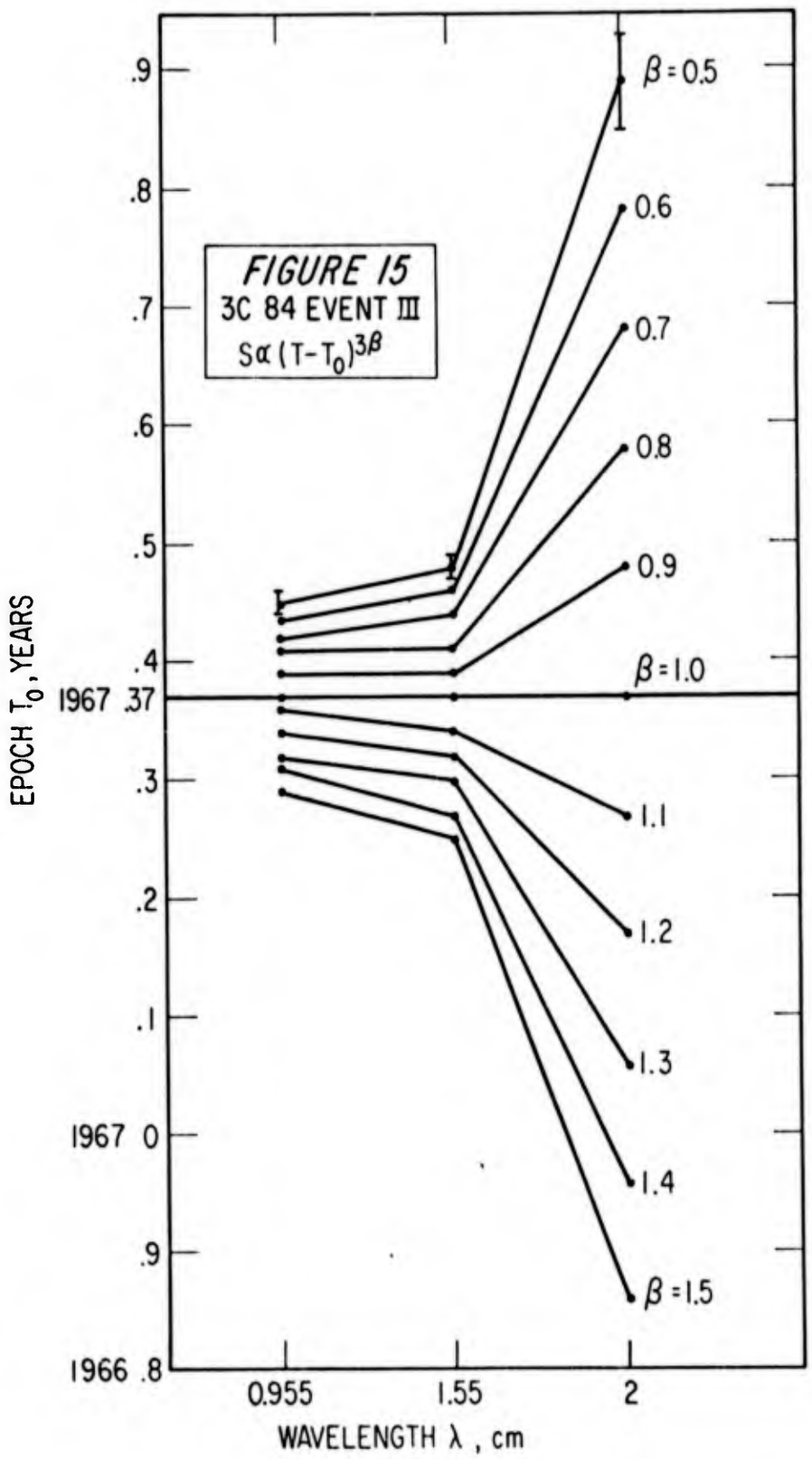
FIGURE 15
3C 84 EVENT III
$S \propto (T-T_0)^{3\beta}$
$\beta = 0.5$
0.6
0.7
0.8
0.9
$\beta = 1.0$
1.1
1.2
1.3
1.4
$\beta = 1.5$
EPOCH T_0, YEARS
1967 .37
1967 0
1966 .8
.9
.8
.7
.6
.5
.4
.3
.2
.1
.9
0.955
1.55
2
WAVELENGTH λ , cm

With these results, and the flux density data at the three wavelengths, γ is found, from equation (42), to be 1.1 ± 0.1.

The time at which the flux density reached its maximum at 9.55 mm and 1.55 cm were 1967.6 ± 0.04 and 1967.63 ± 0.04, respectively. Due to the confusion in the 2 cm data a value of T_m cannot be found. Fig. 16 is the plot of the ages of these maxima along with the predicted slope of 0.49 ± 0.01.

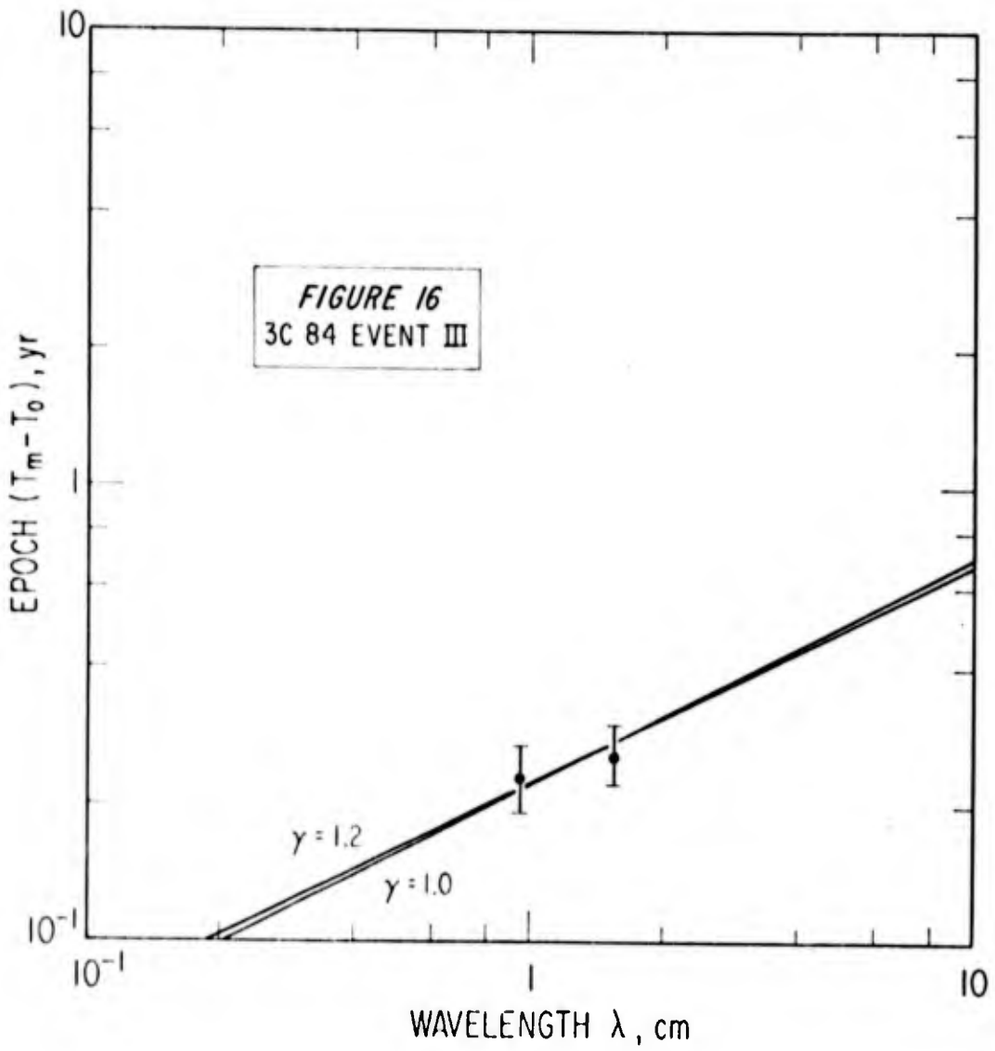

The values of these maxima and the value of the flux density at 2 cm at the extrapolated time its maximum should have occured (1967.68) are shown in Fig. 17. The predicted slope from equation (37), -1.03 ± 0.03, is superimposed on this data.

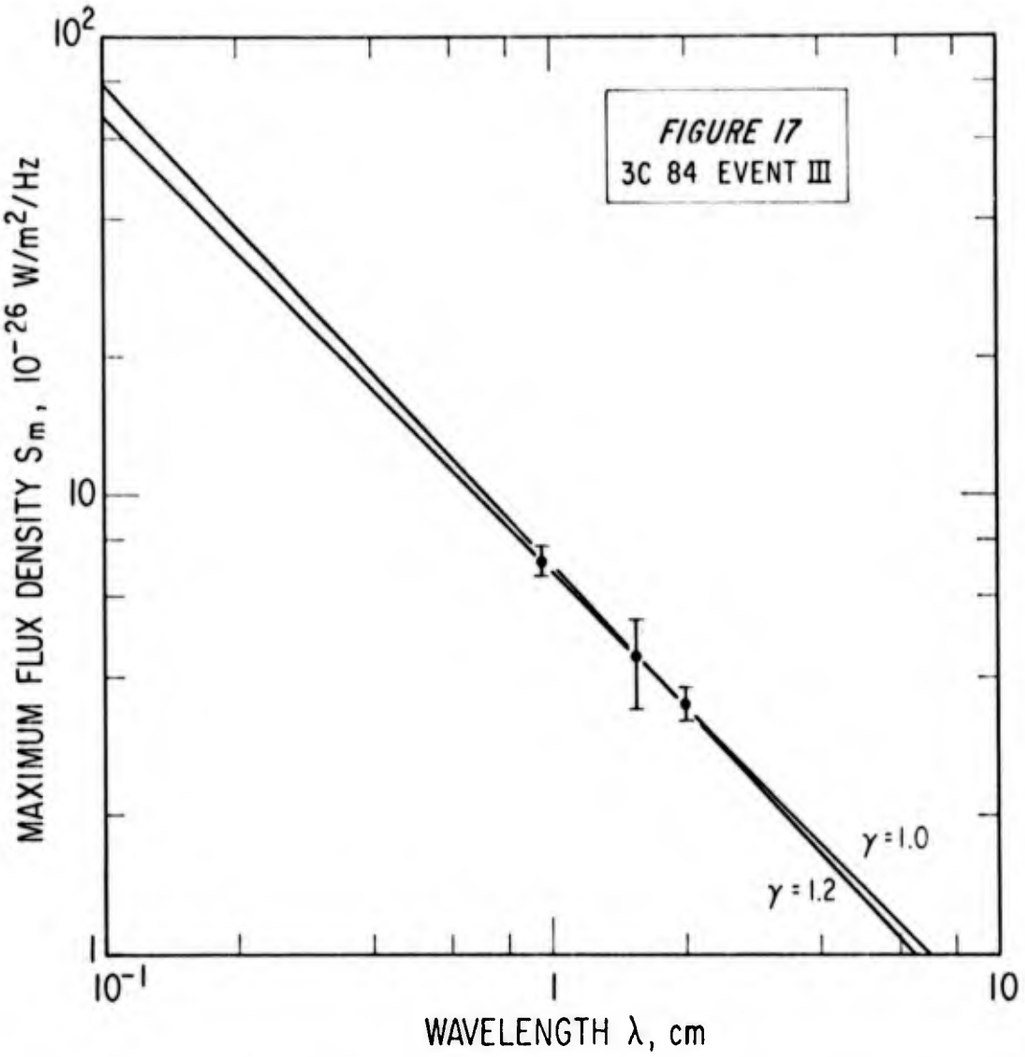

When the flux density reached its maximum value at 1.55 cm the maximum linear size of the source was 3.1 light months, corresponding to 0.0003 arc sec. With ν_t = 3.14 x 10^4 MHz (9.55 mm), the maximum magnetic field strength is found to be 4.8 x 10^{-3} gauss.

The model is successful in describing the three events analyzed. For event I the correlation of the model with the observed variation of t_m with λ and of S_m with λ (Figs. 8 and 9) is excellent; the predicted slopes fall within the error bars of all the data points. The shape of the observed spectrum (Fig. 10) for event I also follows closely the predictions of the model. These same comments are true for event II (Figs. 12, 13,and 14) with the exception of the age of the 9.55 mm maxima (Fig. 12). The model would have this maximum occuring at 1967.01 instead of 1967.6 as shown in Fig. 6. The interpolated curve, drawn through the 9.55 mm data in Fig. 6 might be erroneous. The maximum for event II might have occured earlier and been undetected (the 9.55 mm data is sparse in 1967) and this second peak shown might be due to an additional "minor" event. "Contamination" by this minor event may have caused the observed broadening of the 1.55 cm and 2 cm data.

The ages of the peak flux density at 6 cm as shown in Fig. 8 for event I and on Fig. 12 for event II are both taken from the same peak in Fig. 6. In other words, the observed time of the 6 cm maximum agrees with the predictions for both event I and event II. As found, event I is expanding with a constant velocity, (i.e. $\beta = 1.0$) while event II is decellerating ($\beta = 0.8$). This does not preclude the possibility that the expansion velocity of event II is greater than that of event I. It is suggested that

both event I and event II reached optical transparency at 6 cm simultaneously. If this is the case, the peak at 6 cm is the sum of the peaks from each event. Indeed, the value of the one maximum from Fig. 6, corrected only for the quiescent component is used for both event I and event II as shown on Figs. 9 and 13. The measured maximum is high in both cases; half this value would provide a good fit in both cases. There is no 3.3 mm point for the 1967.4 spectrum in Fig. 14 because the event was over at 3.3 mm by this time.

Event III is not observed as completely as event I or event II, but as shown in Figs. 16 and 17, the predictions of the model do satisfy the observed behavior. In fact, of the three events, number III shows the best correlation with the model.

It was shown in section three that the effects of an event are seen first at the highest frequency and then at later times at lower frequencies. In Fig. 6 activity (possible events) can be seen in the 3.3 mm data. It will be interesting to see if these variations show up at the longer wavelengths in the future. Certainly observers should be on the alert to look for them.

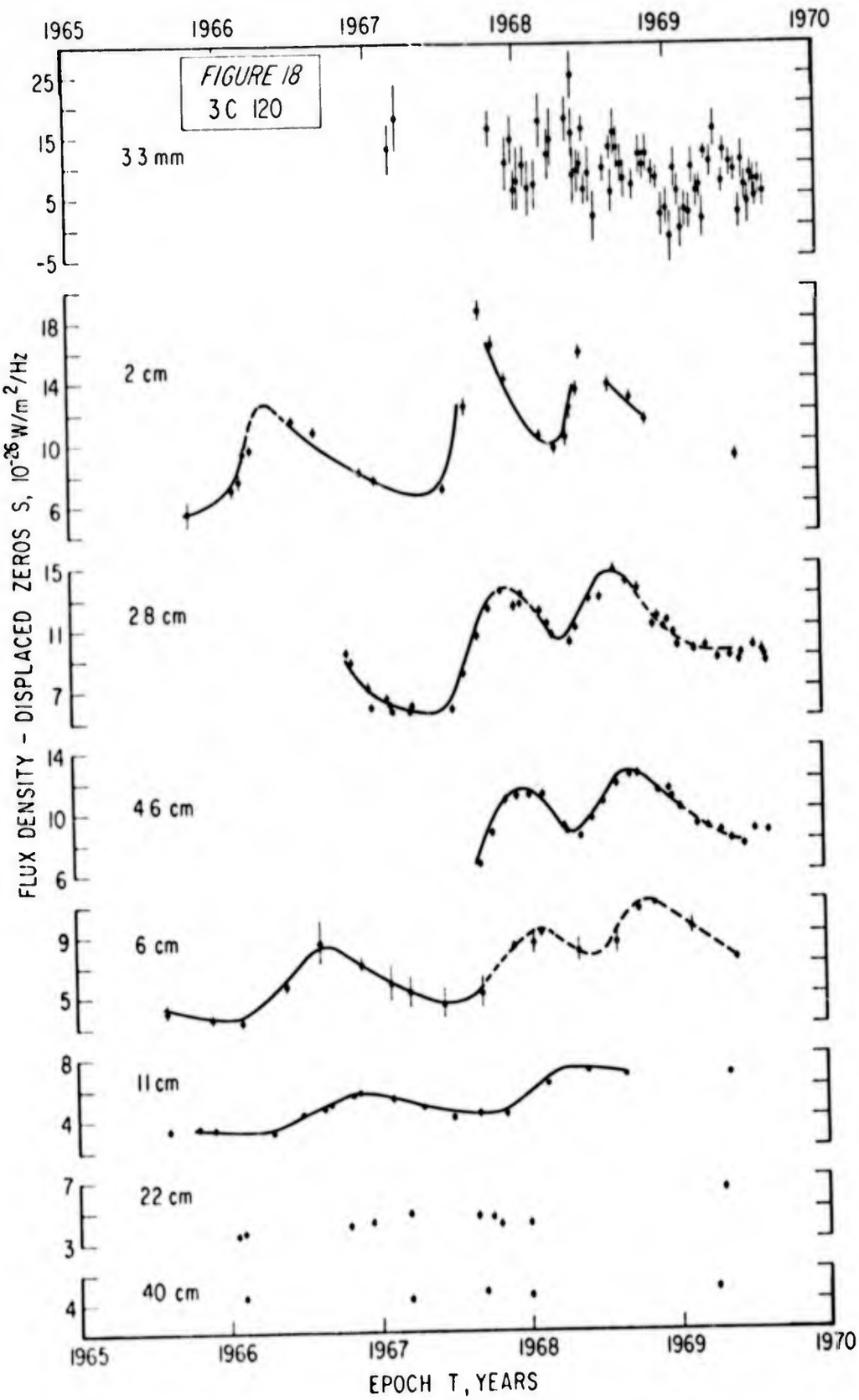
FIGURE 18
3C 120
1965
1966
1967
1968
1969
1970
33 mm
2 cm
28 cm
46 cm
6 cm
11 cm
22 cm
40 cm
FLUX DENSITY - DISPLACED ZEROS S, 10^{-26} W/m^2/Hz
EPOCH T, YEARS

3C 120

3C120 is a Seyfert galaxy with a red-shift equal to 0.0323 (Ref.30:843). Its distance from the earth is therefore approximately 100 Mpc. The data for 3C120 (Fig 18) include observations from wavelengths of 3.3 mm to 40 cm for the period from 1965 to late 1969. Three events are seen to be evolving during this interval. Event I, which was first observed in 1966.1 at 2 cm and then later at 6 and 11 cm, was analyzed, with β assumed to be one, by Pauliny-Toth and Kellerman (Ref.34:L169-L175). No observations were made at 3.3 mm from 1967.22 until 1967.84, with the result that the maximum flux density due to event II was missed at this wavelength. The effect of event II is, however, clearly seen at 2, 2.8, 4.6, 6 and 11 cm. Event III was observed from 3.3 mm in 1968.3 to 6 cm in 1968.8. The quiescent components at 2 cm, 2.8 cm, 6 cm, and 11 cm were slowly increasing with mean values of approximately 7, 5.8, 5.9, 3.5, and 3.4 flux units respectively. The quiescent component at 3.3 mm appears to have been steady at 2 flux units or slightly decreasing.

Event II. The well defined increases in flux density at 2, 2.8, 4.6, and 6 cm are used with equation (41) to determine $T_o = 1967.38 \pm 0.04$ and $\beta = 1.0$ (see Fig. 19). T_o is in excellent agreement with the value of 1967.38 ± 0.05 found by Pauliny-Toth and Kellerman (Ref.34:L172). From equation (42) a value of γ consistent with the flux density decline at 3.3 mm, 2, 2.8, and 4.6 cm is found

to be 1.0 ± 0.1.

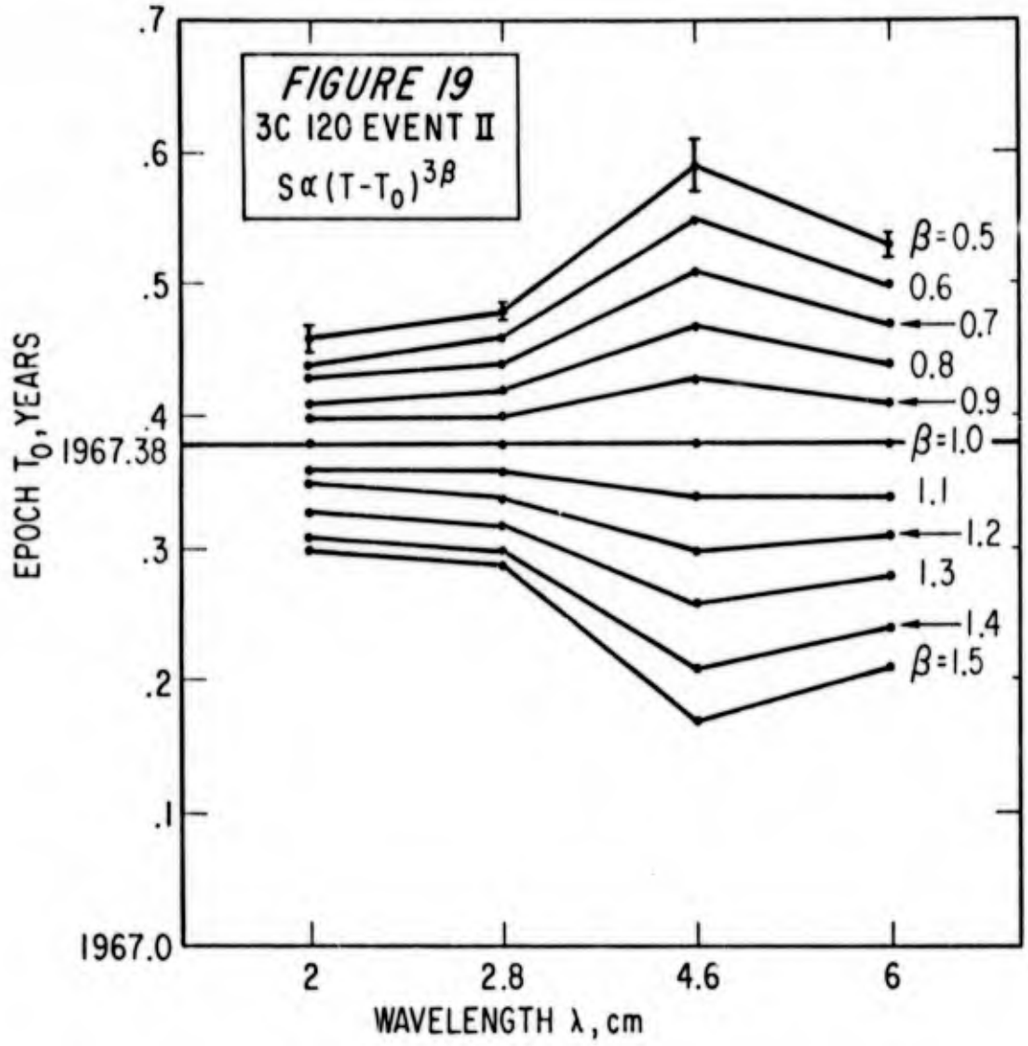

From Fig. 18 the epochs of the maxima are 2 cm- 1967.78, 2.8 cm - 1967.91, 4.6 cm - 1968.02 and 6 cm - 1968.11. The ages of these maxima as well as the slope (0.5 ± 0.01) predicted by equation (40) for γ = 1.0 ± 0.1 are plotted in Fig. 20. Fig. 21 is the values of the flux density maxima versus wavelength together with the slope of - 1.0 ± 0.03 as predicted by equation (37).

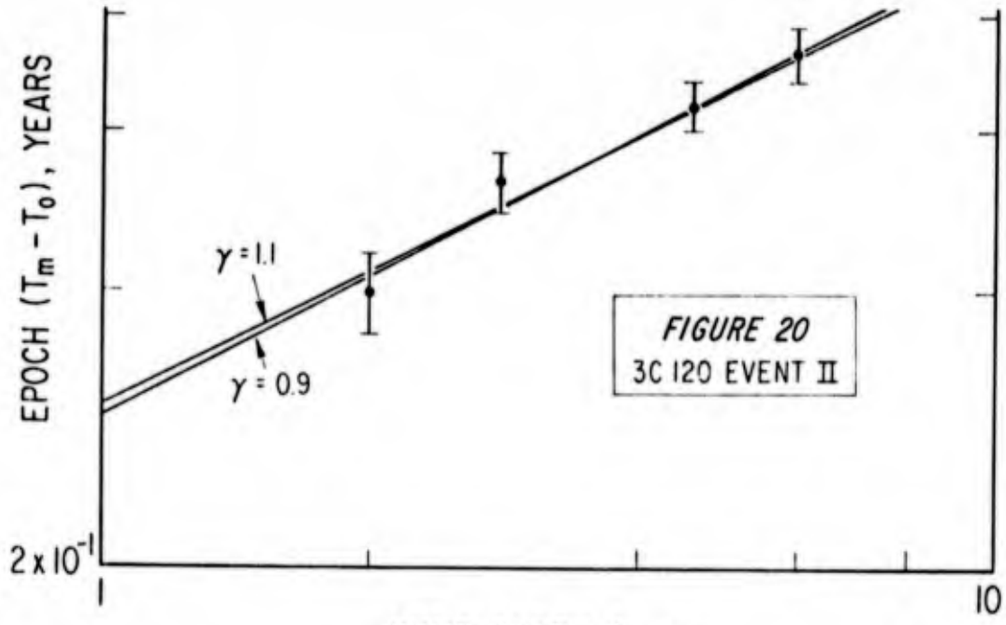

FIGURE 20
3C 120 EVENT II

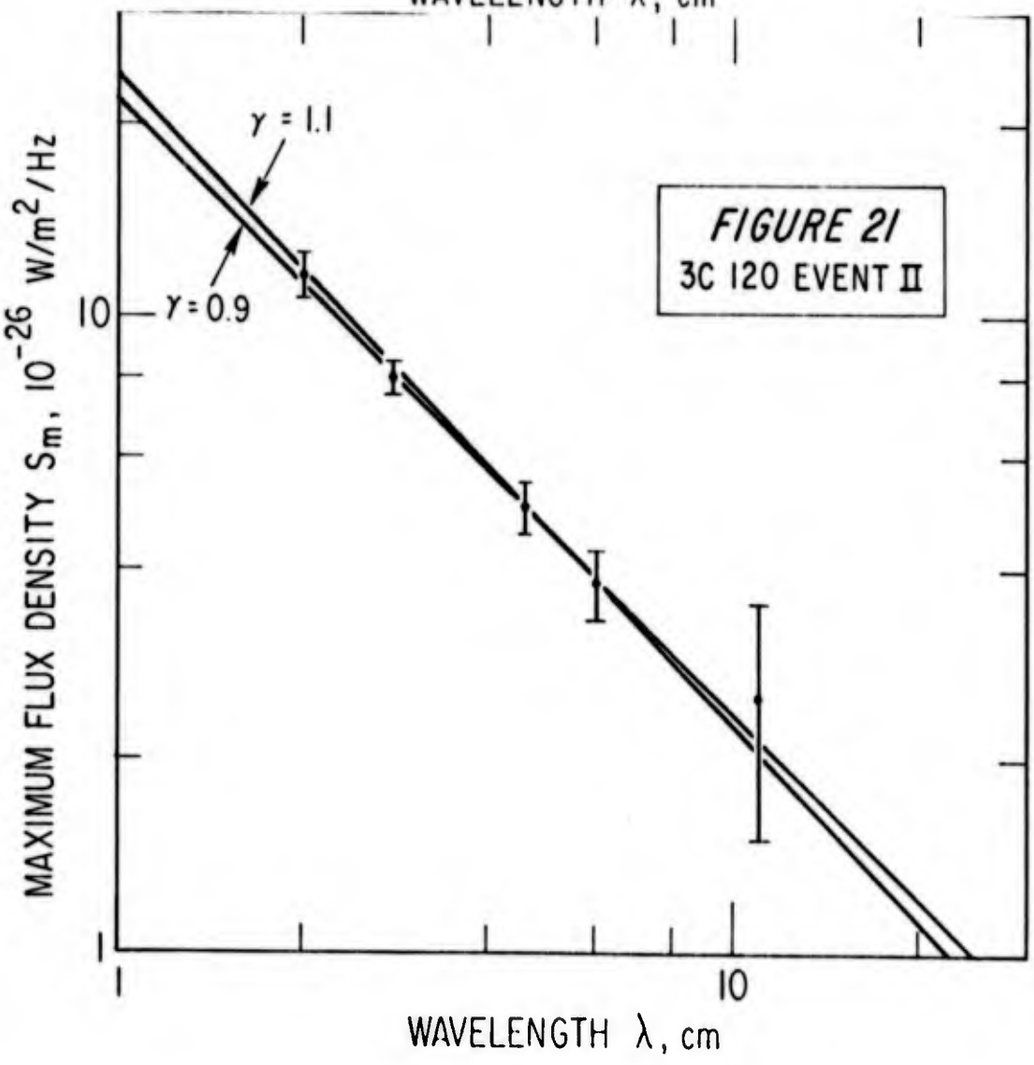

FIGURE 21
3C 120 EVENT II

The spectra of event II for the epochs 1967.5, 1967.7, 1967.9, 1968.1 and 1968.3 are shown in Fig. 22. The expected slopes of 2.5 (eq 35) and 0.0 ± 0.05 (eq 36) are shown best fitted with the data. The dotted points at 3.3 mm (9.08×10^4 MHz) indicate an extrapolation from the available 3.3 mm data. Excellent correlation is obtained.

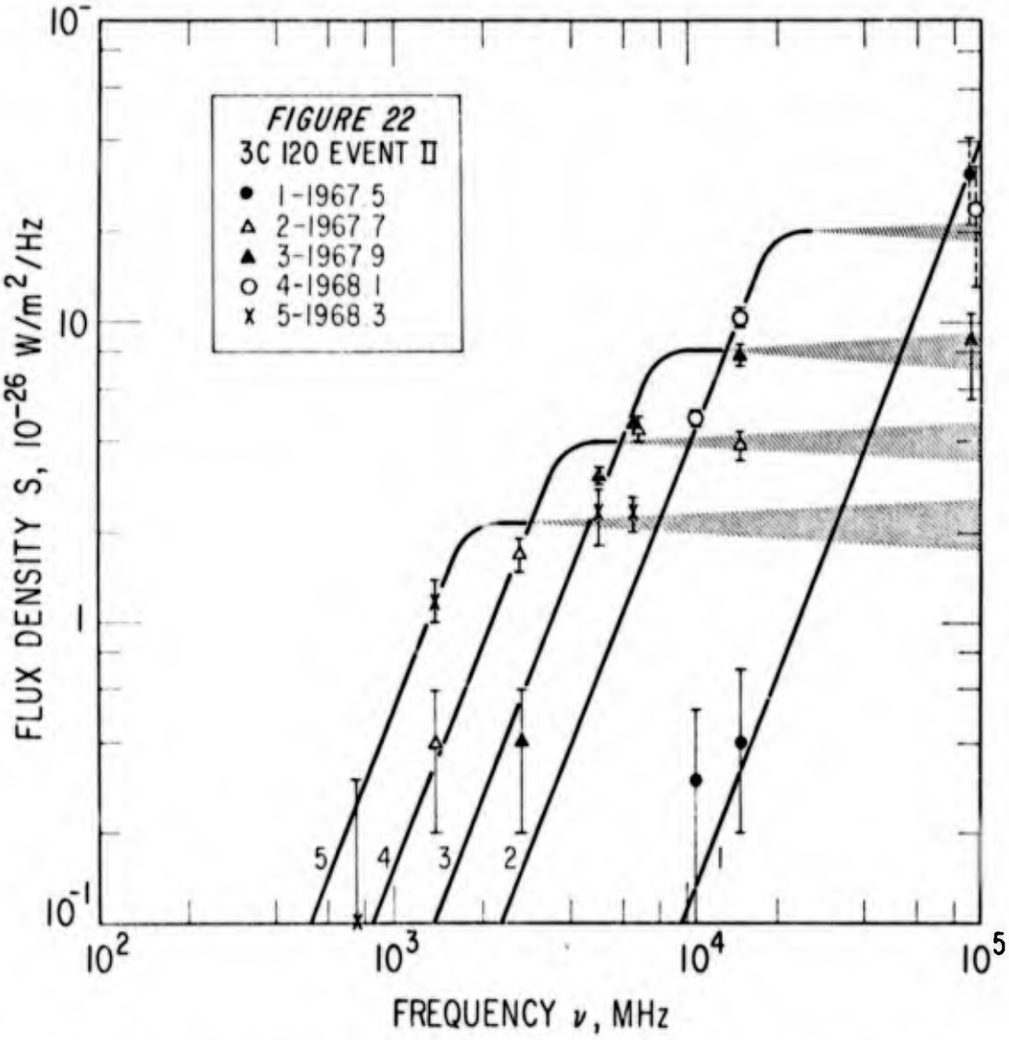

The maximum linear extent of this event when the flux density peaks at 2.8 cm is 6.4 arc sec. With $\nu_t = 1.5 \times 10^4$ MHz (2 cm), the value of the maximum magnetic field strength was 1.3×10^{-4} gauss.

Event III. As shown in Fig. 23 data at 3.3 mm, 2, 2.8, 4.6, and 6 cm are used in equation (41) to find T_o = 1968.07 ± 0.02 and β = 1.0. The decays in flux density at these same wavelengths are used with equation (42) to find γ = 1.2 ± 0.1.

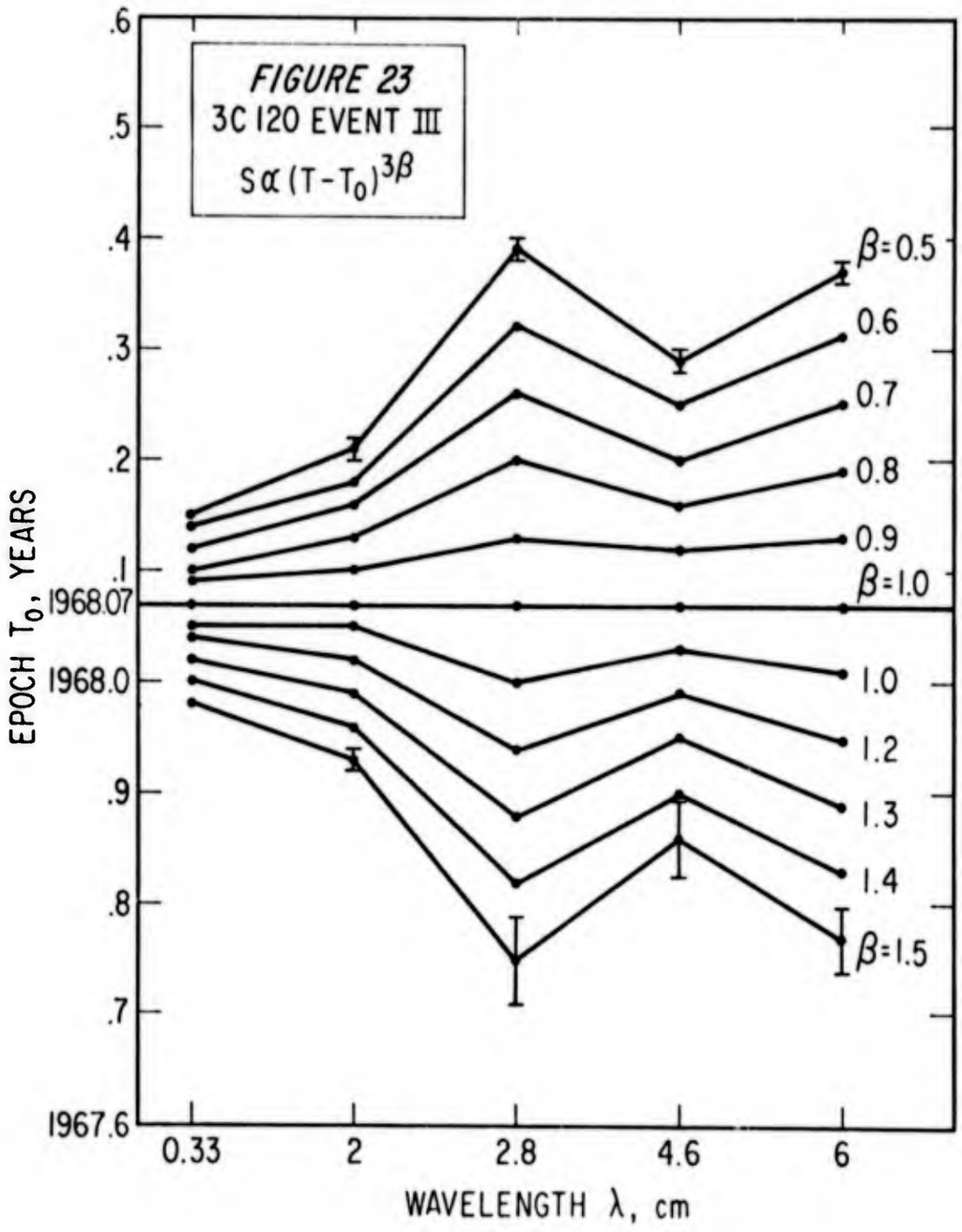

The flux densities reached maxima, for event III, in 1968.32, 1968.45, 1968.64, 1968.73 and 1968.84 at the wavelengths of 3.3 mm, 2 cm, 2.8 cm, 4.6 cm and 6 cm, respectively. The corresponding ages and the predicted slope of 0.48 ± 0.008 are shown in Fig. 24. The maximum flux densities reached at these wavelengths together with the predicted slope of - 1.06 ± 0.03 from equation (37) are shown in Fig. 25. The 3.3-mm value falls 57 flux units short of the predicted values.

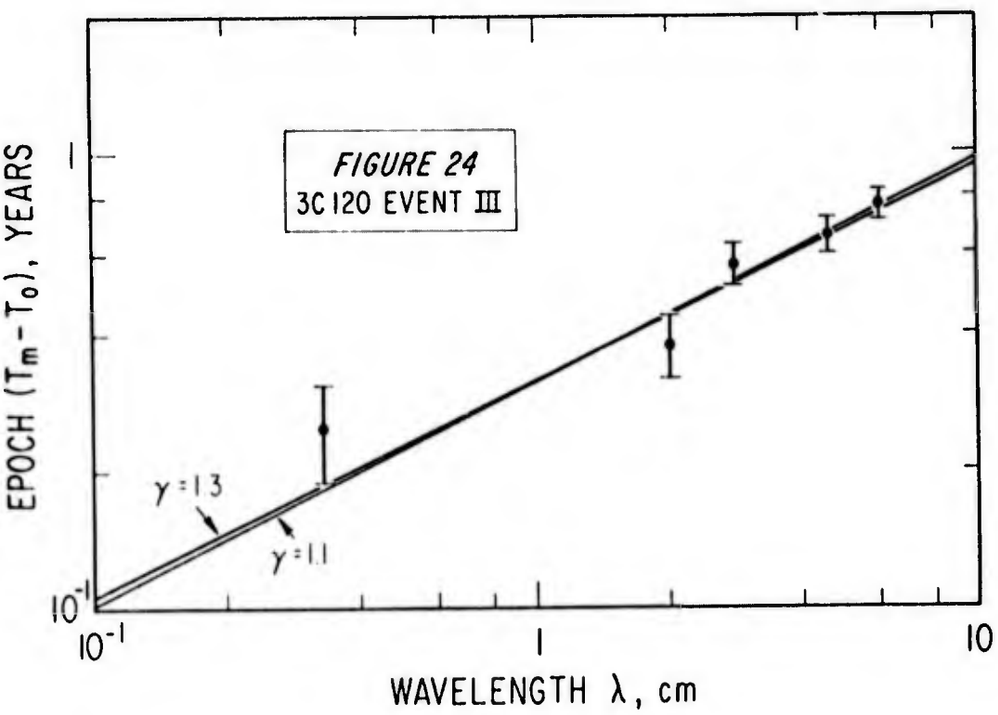

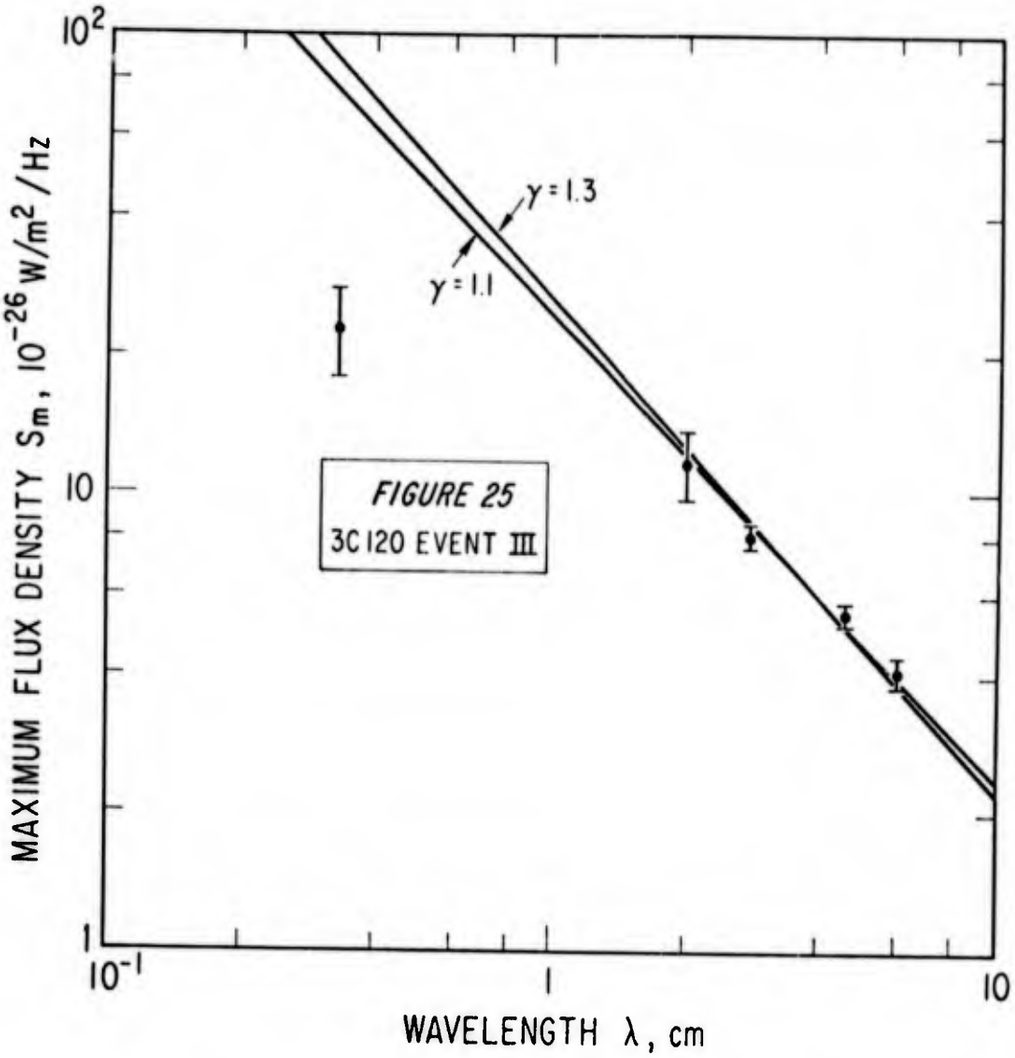

The spectra of event III for the epochs 1968.4, 1968.6 and 1968.8 and the expected slopes of 2.5 (eq 35) and -0.1 $\pm$0.05 (eq 36) are shown in Fig. 26 in good agreement.

When the flux density peaked at 2.8 cm, the maximum linear size of the source was 6.8 light months and the maximum angular size was 0.0004 arc sec. The maximum magnetic field strength using ν_t = 1.07 x 10^4 MHz in equation (43) was 1.7 x 10^{-4} gauss.

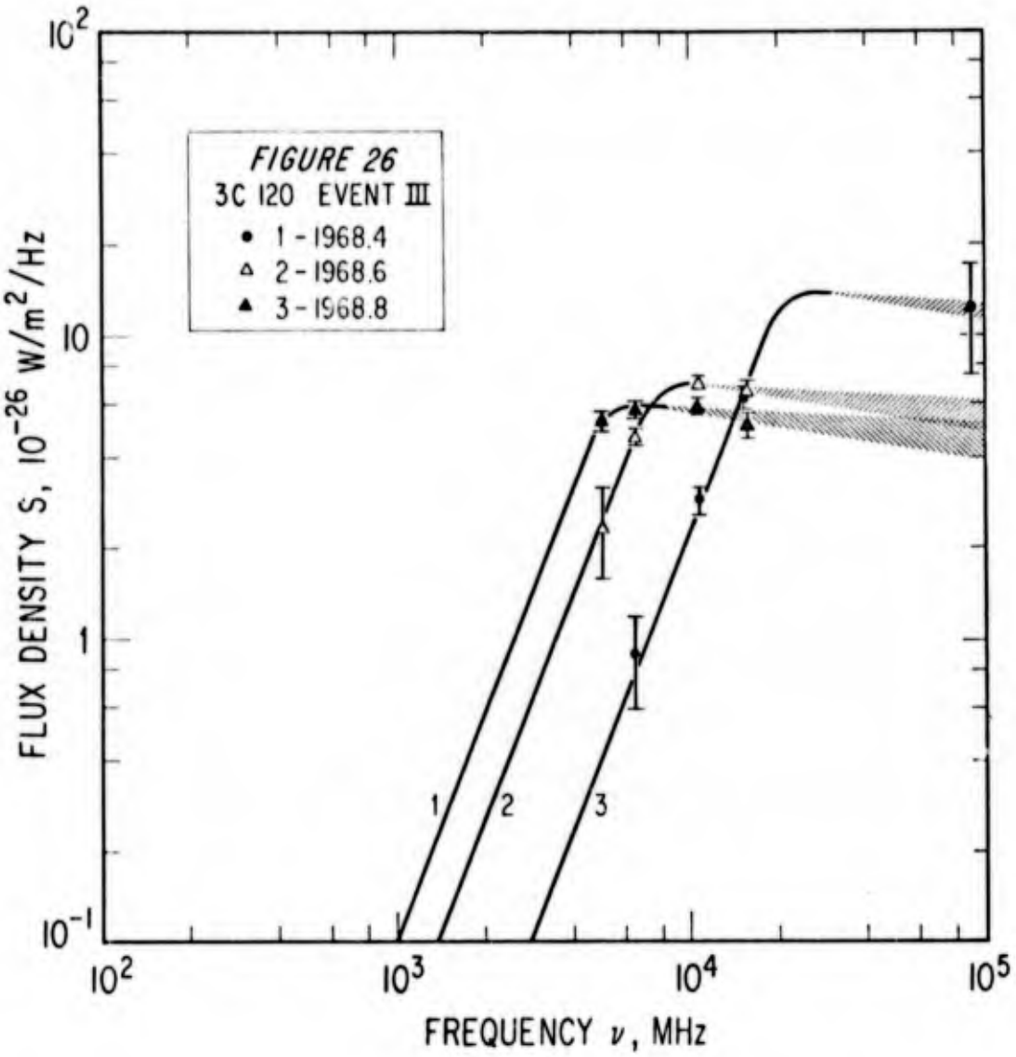

The correlation of the predicted functional relations of t_m with λ, S_m with λ, and S with ν with the observed behavior for event II are excellent (see Fig. 20, 21 and 22). In Fig. 22 the dashed points at 3.3 mm indicate that these values were extrapolated from the existing 3.3 mm data. The effect of event II at 3.3 mm had decayed to the quiescent level by 1968.1; therefore there are no 3.3 mm points for the 1968.1 and 1968.3 spectra in Fig. 22.

Although there is noticeable scatter in the t_m vs λ plot for event III (Fig. 24), there is still good correlation with the predicted trend. The S_m vs λ plot for event III (Fig. 25) shows excellent correlation with the model for the longer wavelengths, but the 3.3 mm point falls approximately 57 flux units short of the predicted value. This is possibly due to energy loss mechanisms, such as inverse compton scattering, which may be acting while the electron cloud is still relatively dense. The spectra of event III (Fig. 26) shows a high correlation with the model. The 3.3 mm value for the 1968.4 spectrum shows good agreement. If there are other energy loss mechanisms at work at 3.3 mm, either it has become less dominant than the expansion by 1968.4 or it was such that it affected only the peak of the outburst and not its general shape away from the peak. Event III is over, at 3.3 mm, before 1968.6; therefore there are no 3.3 mm points for the 1968.6 and 1968.8 spectra.

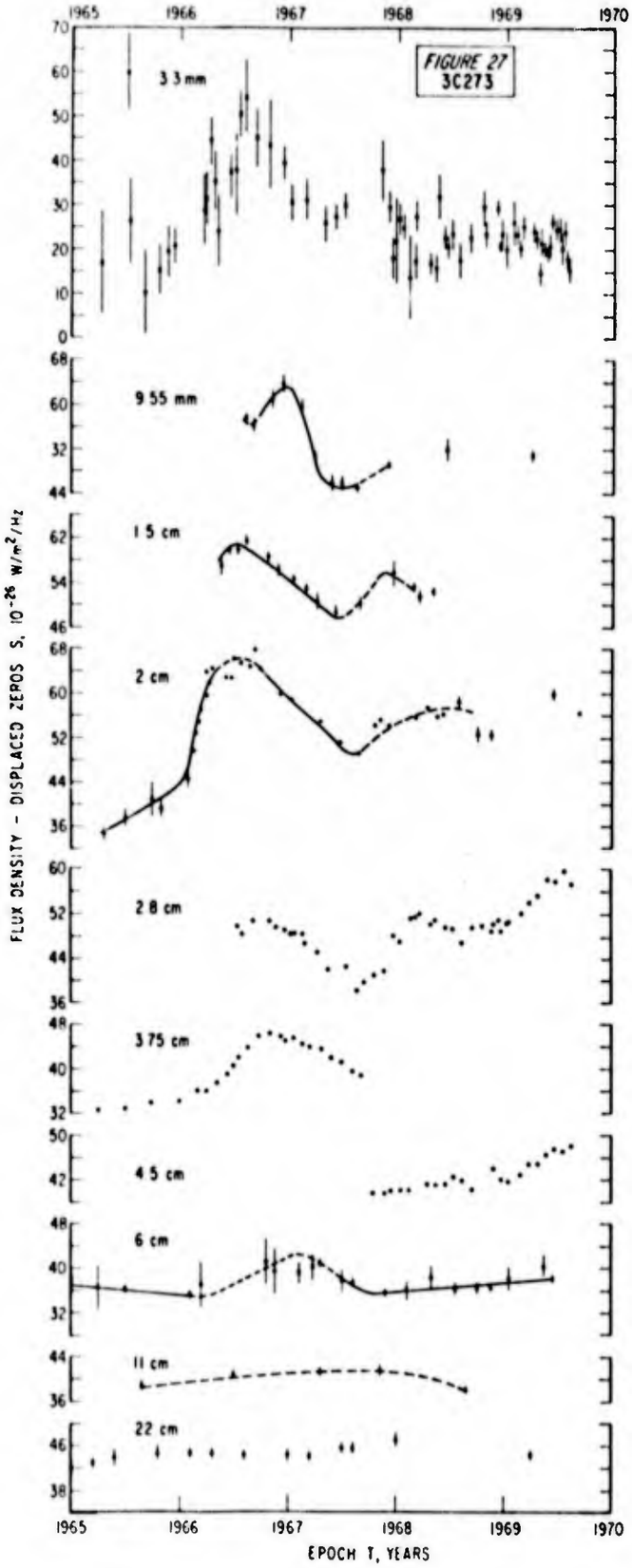
FIGURE 27
3C273
3.3 mm
9.55 mm
1.5 cm
2 cm
2.8 cm
3.75 cm
4.5 cm
6 cm
11 cm
22 cm
1965
1966
1967
1968
1969
1970
FLUX DENSITY - DISPLACED ZEROS S, 10⁻²⁶ W/m²/Hz
EPOCH T, YEARS

3C 273

3C273 is a quasi-stellar radio source with a redshift of 0.158 (Ref.2:739). It is, therefore, approximately 470 Mpc distant. The data for 3C273 (see Fig.27) include observations from 1965 to late 1969. Two major events are clearly displayed during this period with the 3.3 mm data showing at least four events. Analysis of the rises in flux density at each wavelength indicates that the first event is evolving much more slowly than the second event, with the result that, at wavelengths equal to and greater than 9.55 mm, event II is seen first, followed, with increasing delay, by event I. At 3.3 mm the events are in the expected order, i.e., event I causing the increase in flux density at 1965.5 and event II showing up at 1966.28. At 9.55 mm however, the increase in flux density at 1966.8 is due to event I while the effect of event II occured before any observations were made, i.e. before 1966.6. The crossover in time of the two events occured somewhere between 3.3 mm and 9.5 mm. At wavelengths greater than 9.55 mm the first increase in flux density is due to event II while the second is due to event I. The effect of any of the other events, seen at 3.3 mm, have not yet become apparent at the longer wavelength, with the exception of the 1967.8 increase at 9.55 mm. The quiescent components were taken to be approximately 10 flux units at 3.3 mm, 42 flux units at 9.55 mm, 46 flux units at 1.55 cm, 30 rising to 44 flux units at 2 cm,

approximately 34 flux units at 2.8 cm, 32 flux units at 3.75 cm and 34 flux units at 6 cm.

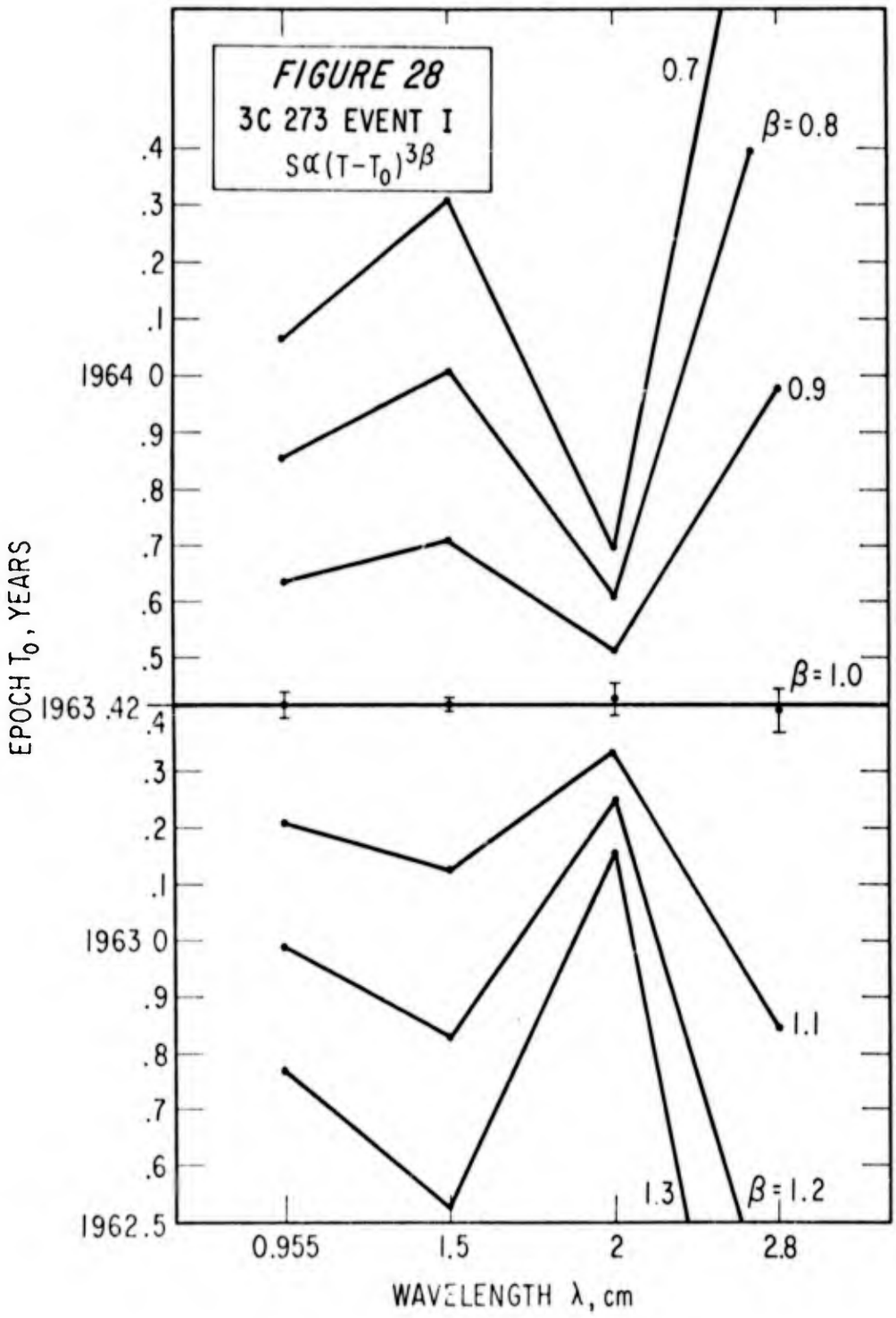

Event I. Fig. 28 is the result of the evaluation of equation (41) at 9.55 mm, 1.5 cm, 2 cm, and 2.8 cm. The 3.3 mm data, which definitely reflects the effect of event I, is too sparce to analyze accurately. T_o is found to be 1963.42 $\pm$ 0.01 and $\beta = 1.0$. From equation (42) γ, consistent with the decay of flux density at 3.3 mm, 9.55 mm, and 1.5 cm, is found to be 1.3 $\pm$ 0.1.

The epochs of maximum flux density at 3.3 mm, 9.55 mm, 1.5 cm, 2 cm and 2.8 cm are, from Fig. 27, 1965.6, 1967.0, 1968.11, 1967.6 and 1969.6 respectively. The corresponding ages versus λ and a slope of 0.473 $\pm$ 0.008, from equation (40) are shown in Fig. 29. The magnitude of these maxima versus λ and a slope of 1.08 $\pm$ 0.02 from equation (37) are shown superimposed in Fig. 30.

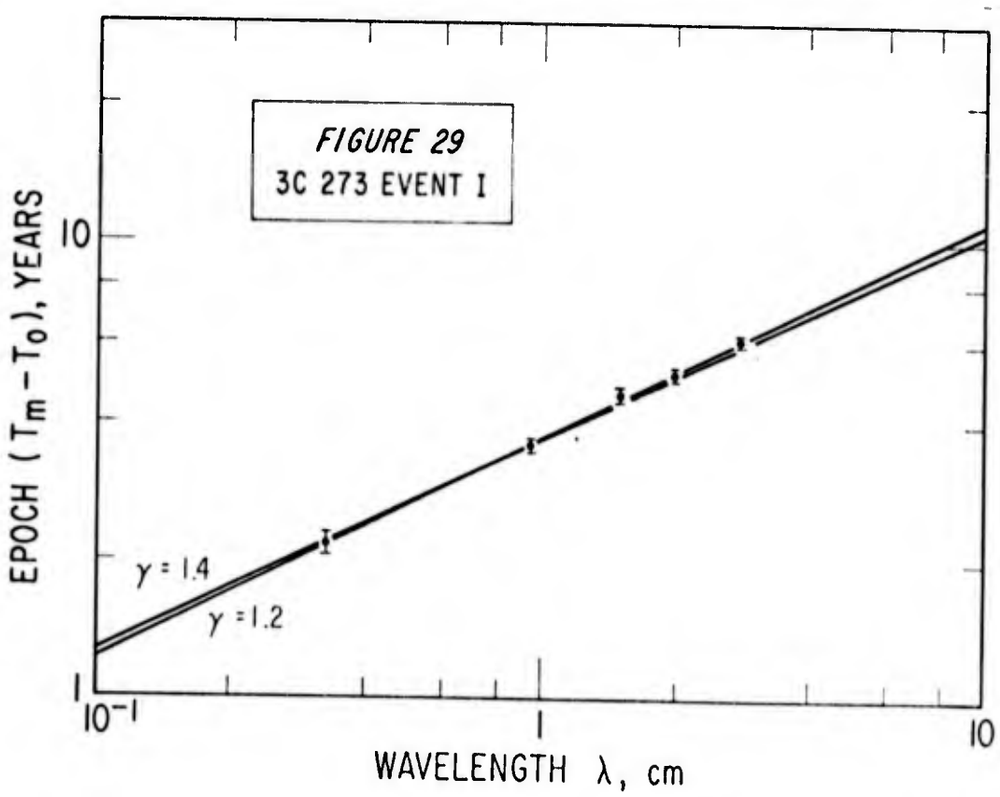

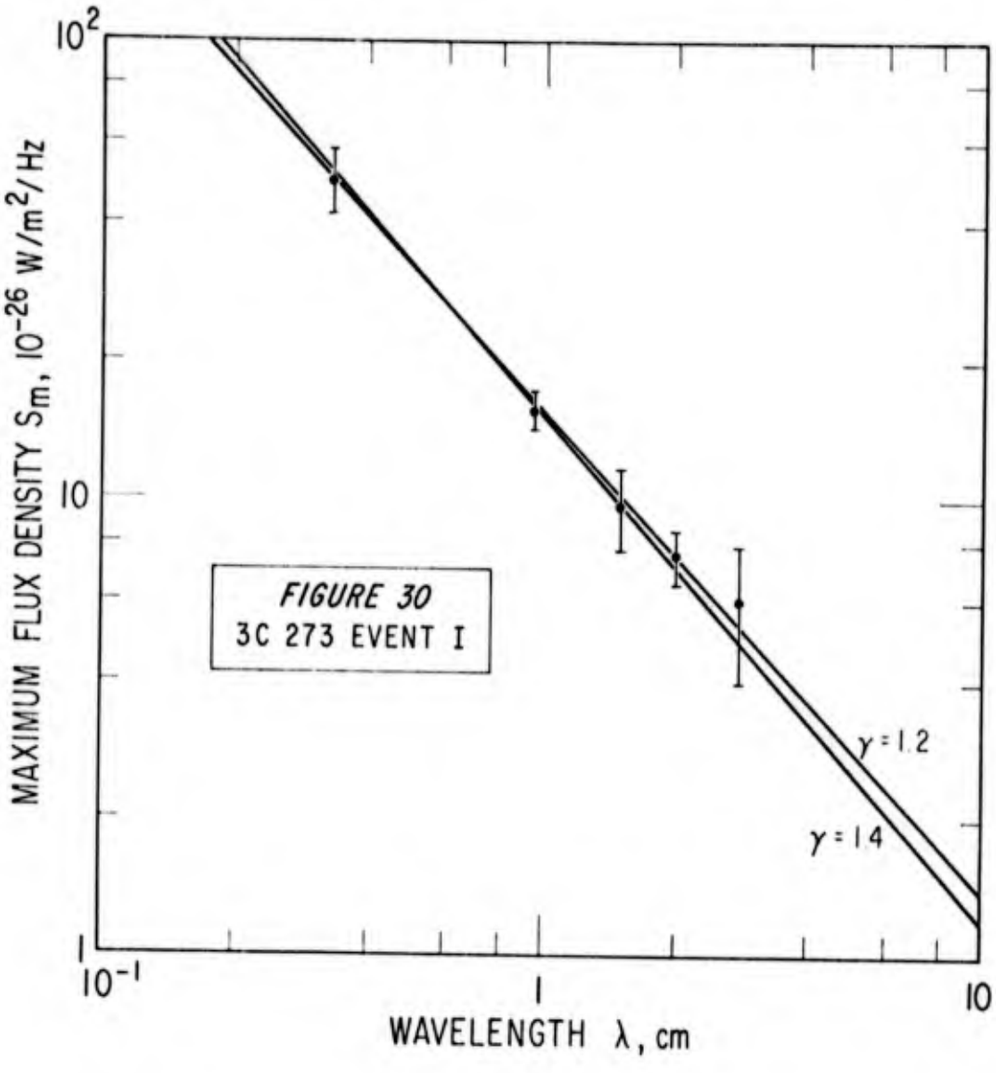

At the epoch 1969.6 when the flux density peaked at 2.8 cm, the maximum linear extent was six light years, corresponding to an angular size of 0.0008 arc sec. Using $\nu_t = 1.5 \times 10^4$ MHz, equation (43) yields a maximum magnetic field strength of 9.5×10^{-3} gauss.

Event II. Equation (41) is evaluated with flux density measurements at wavelengths of 3.3 mm, 1.5 cm, 2 cm, 3.75 cm and 6 cm (see Fig. 31). Values for T_o and β are 1965.82 $\pm$ 0.02 and 1.2 respectively.

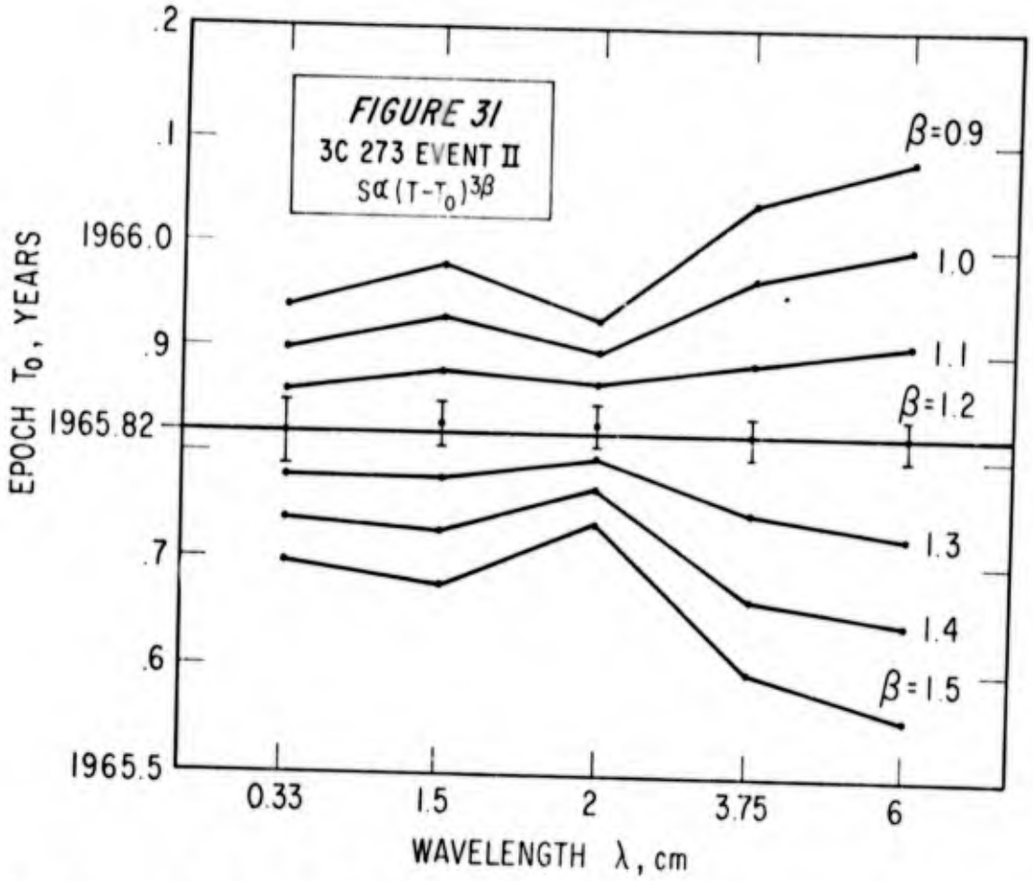

From equation (42) a value for γ consistent with the observations at 3.3 mm, 1.5 cm, 2 cm, 2.8 cm, 3.75 cm and 6 cm is found to be 1.6 ± 0.1.

There are two possible peaks at 3.3 mm due to event II, with times of 1966.22 and 1966.6. The ages of both of these maxima and the maxima occurring at 1.5 cm in 1966.54, 2 cm in 1966.6, 2.8 cm in 1966.7, 3.75 cm in 1966.85 and 6 cm in 1967.1, along with a slope of 0.375 ± 0.005 from equation (40), are shown in Fig. 32.

From the correlation of the longer wavelength data with the predicted slope it is concluded that the 1966.22 peak at 3.3 mm is the proper one to be associated with event II.

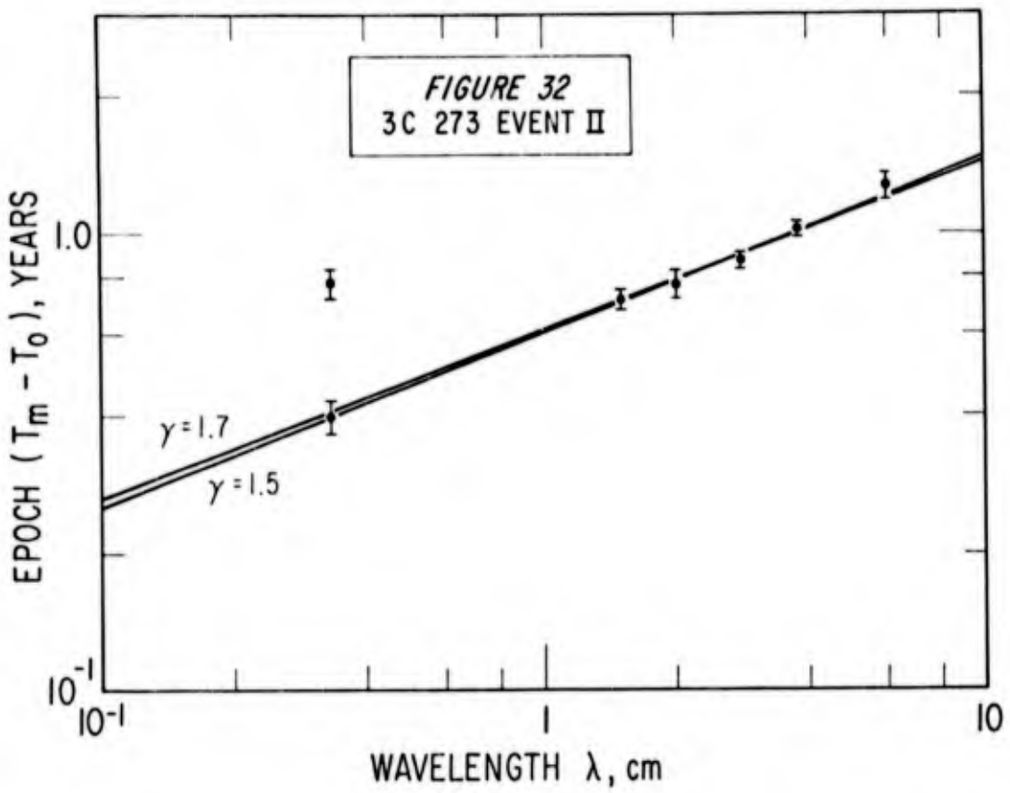

In Fig. 33 are presented the flux density values of these maxima and the predicted slope of - 1.145 ± 0.02 from equation (37). The 3.3 mm value is 150 flux units lower than the value expected by the correlation of the longer wavelength data with the model. This is consistent with a similar result found by Simon (Ref. 39).

The spectra of event II for the epochs 1966.2, 1966.4, 1966.6, 1966.8 and 1970.0 are shown in Fig. 34. The slopes indicated are those predicted by the model, 2.5 (eq 35) and - 0.3 ± 0.05 (eq 36). Again, the 3.3 mm point near the time of the maximum falls far short of the expected value of the 1966.2 spectrum.

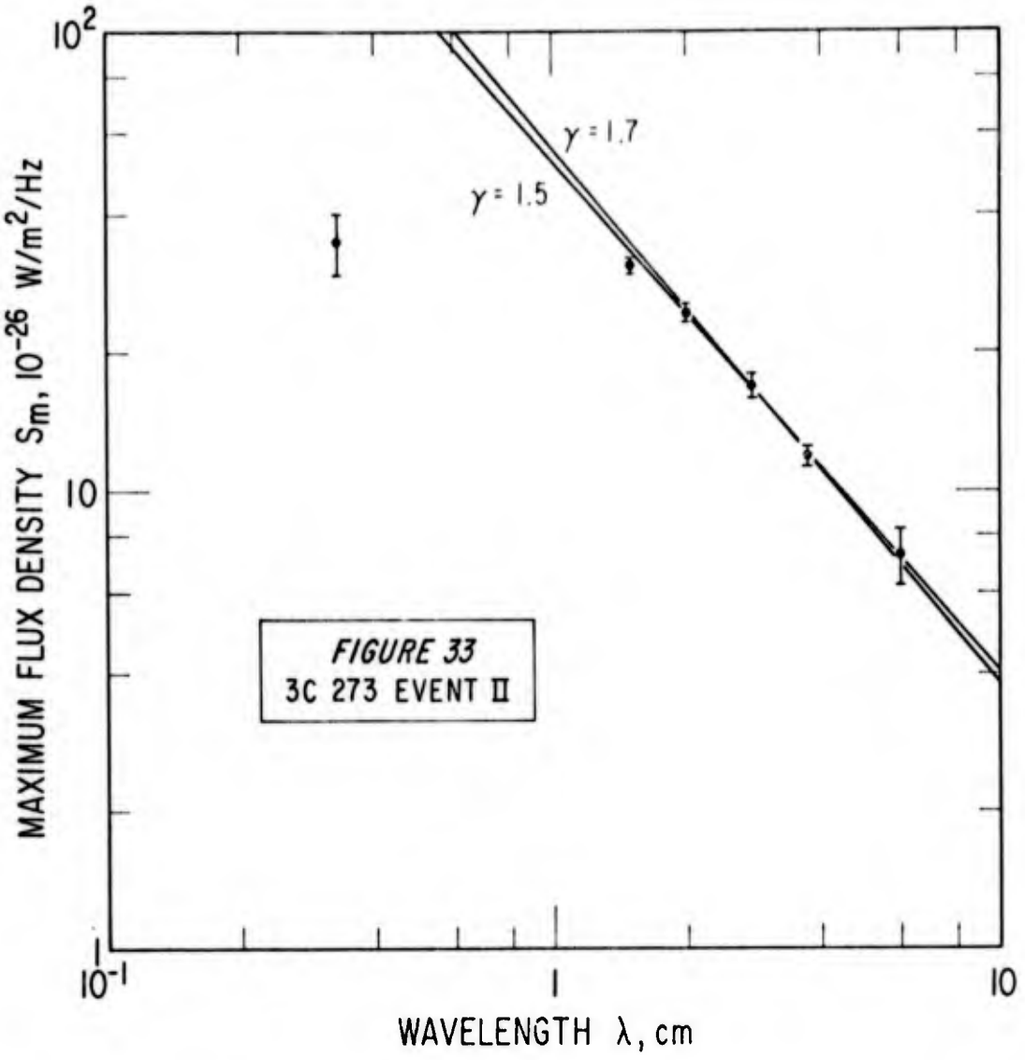

FIGURE 33
3C 273 EVENT II

The maximum linear extent of the source in 1966.7 was 10.6 light months and with R = 470 Mpc the maximum angular size was 0.0001 arc sec. With $\nu_t = 1.5 \times 10^4$ MHz the maximum magnetic field strength, from equation (43) was 6.7×10^{-7} gauss.

The correlation between the observed variations of t_m vs λ and the predicted variations (Fig. 29) for event I is excellent. Only lines with slopes very close to the predicted one could be drawn through the points.

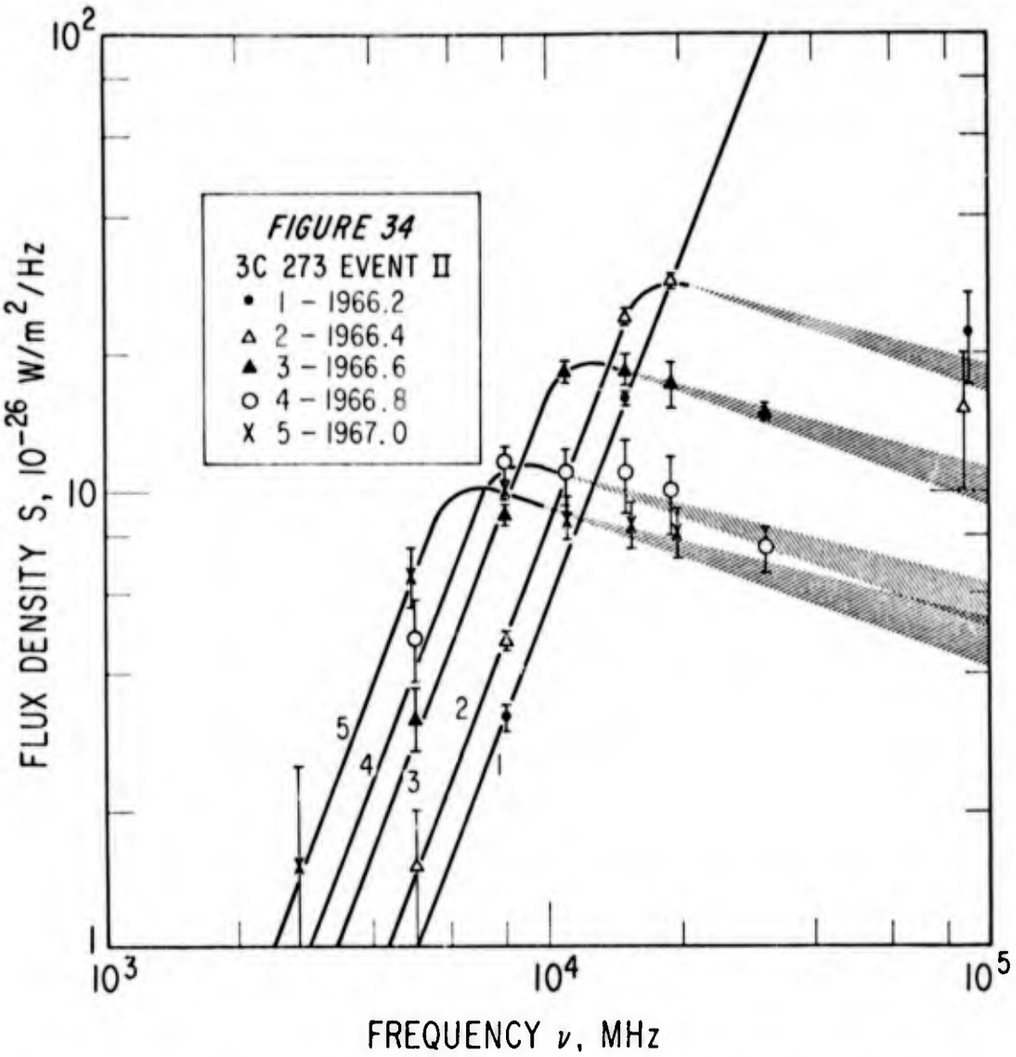

Similarly, the correlation is excellent between the observed S_m vs λ and the prediction (see Fig. 30). Because this event is evolving so slowly, only two wavelengths, at most, manifest the event at any time. For this reason no useful spectrum could be formed. For event II, Fig. 32 shows the excellent degree of correlation between predicted and observed variations of t_m with λ. Two points are shown at 3.3 mm. The one corresponding to t_m = 0.78 years (1966.6 in Fig. 27) was at first assumed to be associated with event II, but extrapolation from the longer wave -

length data shows that the correct peak occurred in 1966.22 ($t_m = 0.4$). The evaluation of T_o and β (Fig.31) by using what was thought to be the leading edge of the 1966.6 peak is not in error, for two reasons. First, even if the 3.3 mm results are ignored in Fig. 31, the longer wavelength results still yield the same T_o and β. Second, the data used at 3.3 mm were taken so much earlier than the 1966.6 peak that they were the leading edge of the 1966.22 peak.

The S_m vs λ plot for event II (Fig. 33) shows excellent correlation at the longer wavelengths, but a deviation from the prediction starts at 1.5 cm and increases until, at 3.3 mm, the observed value is approximately 150 flux units below the value predicted by extrapolating the longer wavelength data to 3.3 mm. Similarly, in the spectrum of event II (Fig. 34) for the epoch 1966.3, the 3.3 mm point falls far short of the predicted value. By 1966.3, however, the value of the flux density at 3.3 mm is within the range predicted by the model.

There are no 3.3 mm points for the spectra of 1966.6, 1968.8 and 1970.0 because at 3.3 mm event II has decayed and a new event has begun by 1966.5.

The failure of the model to account for the high frequency flux density value may again be due to the operation of energy loss mechanisms not considered in the model. The effect of the 1966.6 rise at 3.3 mm may have been missed at 9.55 mm and 1.5 cm and may be causing the broadening effect of the 1968 data at 2 cm. The 1968.2

rise at 2.8 cm may be related to the outburst. If this is the case, then there is another crossover in time between event I and this event (III). The order of the event at 3.3 mm is normal, i.e., I, II, III, but at 2.8 cm the order would be II, III, I.

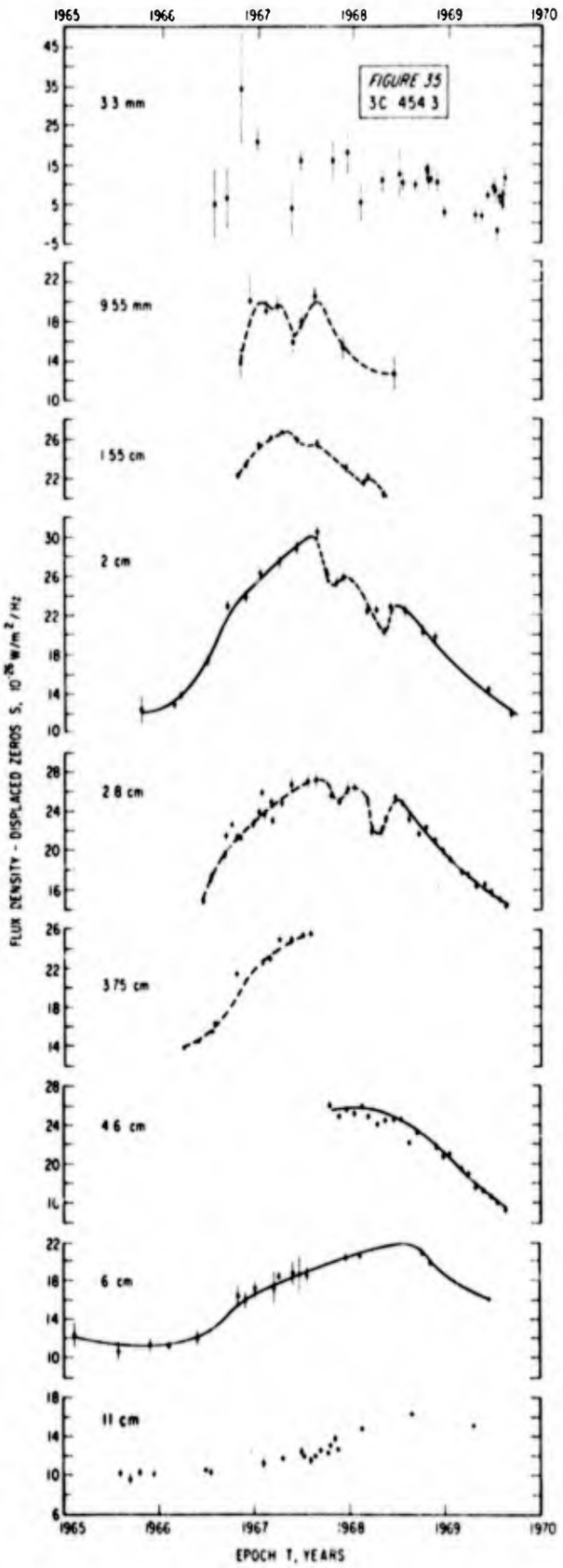
FIGURE 35
3C 454 3
3.3 mm
9.55 mm
1.55 cm
2 cm
2.8 cm
3.75 cm
4.6 cm
6 cm
11 cm
FLUX DENSITY - DISPLACED ZEROS S, 10^{-26} w/m^2/Hz
EPOCH T, YEARS
1965
1966
1967
1968
1969
1970

3C 454.3

3C454.3 is a quasi-stellar radio source with a redshift equal to 0.859 (Ref.2:740). This corresponds to a distance of 2600 Mpc. Fig. 35 is the observed flux density for 3C454.3 at wavelengths from 3.3 mm to 11 cm for the period from 1965 to late 1969. The data indicates the presence of three events during this interval that considerably overlap in time. Event II and III are so confused by the flux density due to event I that analysis of them proved unsuccessful. In fact, the temporal spacing of the three events decrease with time to the point where, at 6 cm they appear as one event. A quiescent level of 0.0. was used at 3.3 mm and approximately 10 flux units at the other wavelengths.

Event I. The increase in flux density at 1.55, 2, 2.8, and 6 cm were used with equation (41) with a resulting value of T_o = 1965.84 ± 0.06 and β = 1.1 (see Fig. 36). A value of γ = 1.1 ± 0.1 was found, (from equation (42)), consistent with the decay in flux density at 1.55 cm, 2 cm 2.8 cm, 4.6 cm and 6 cm.

The flux density peaks were reached in 1967.1 at 9.55 mm, 1967.35 at 1.55 cm, 1967.6 at 2 cm, 1967.7 at 2.8 cm, 1968.1 at 4.6 cm and 1968.6 at 6 cm. The ages of these peaks and a slope, from equation (40), of 0.446 ± 0.008 are shown in Fig. 37. The values of the flux density achieved at these peaks and the predicted slope of -1.03 ± 0.03 from equation (37) are shown superimposed in Fig. 38.

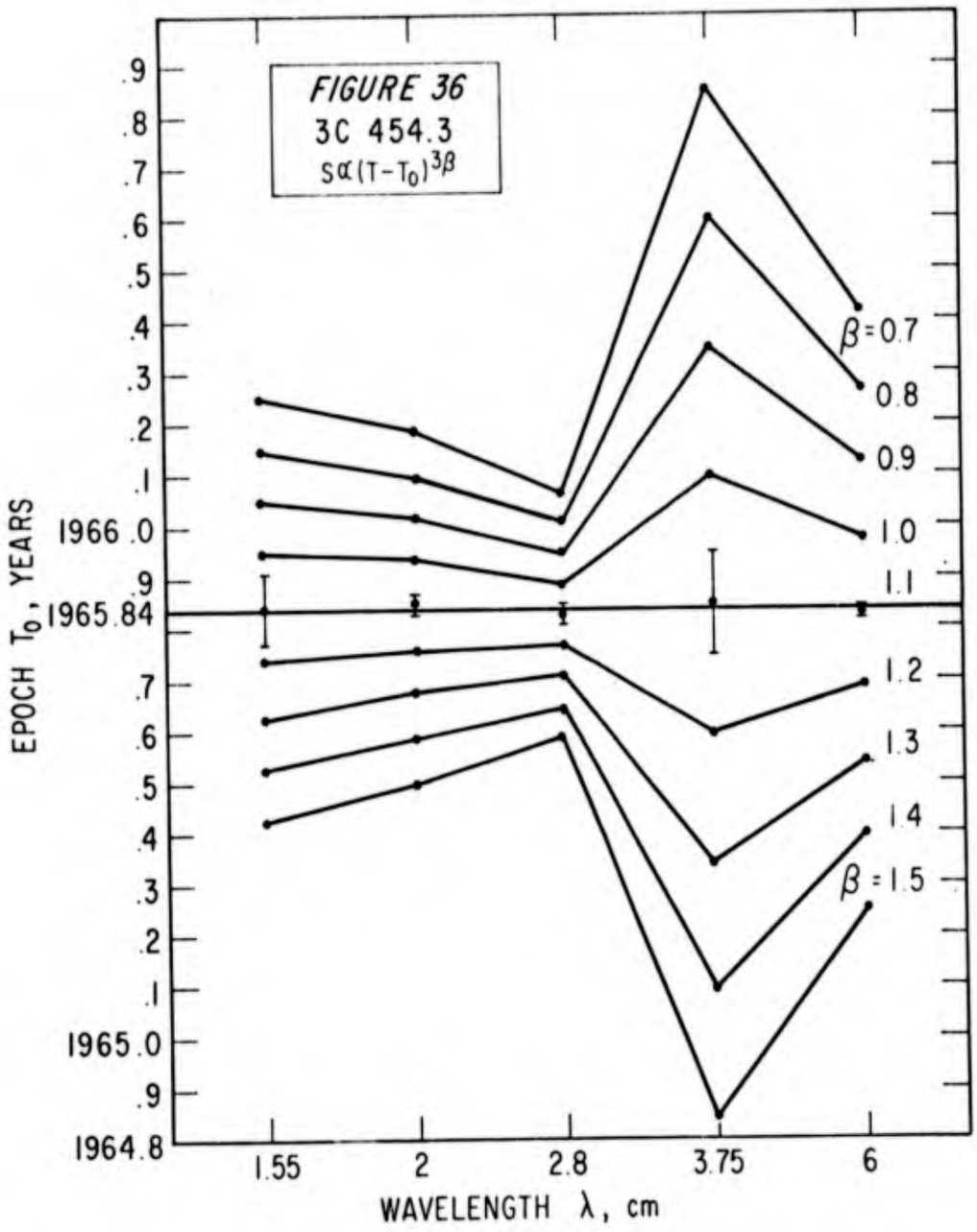
FIGURE 36
3C 454.3
$S\alpha(T-T_0)^{3\beta}$
EPOCH T_0, YEARS
1966.0
1965.84
1965.0
1964.8
.9
.8
.7
.6
.5
.4
.3
.2
.1
β=0.7
0.8
0.9
1.0
1.1
1.2
1.3
1.4
β=1.5
1.55
2
2.8
3.75
6
WAVELENGTH λ, cm

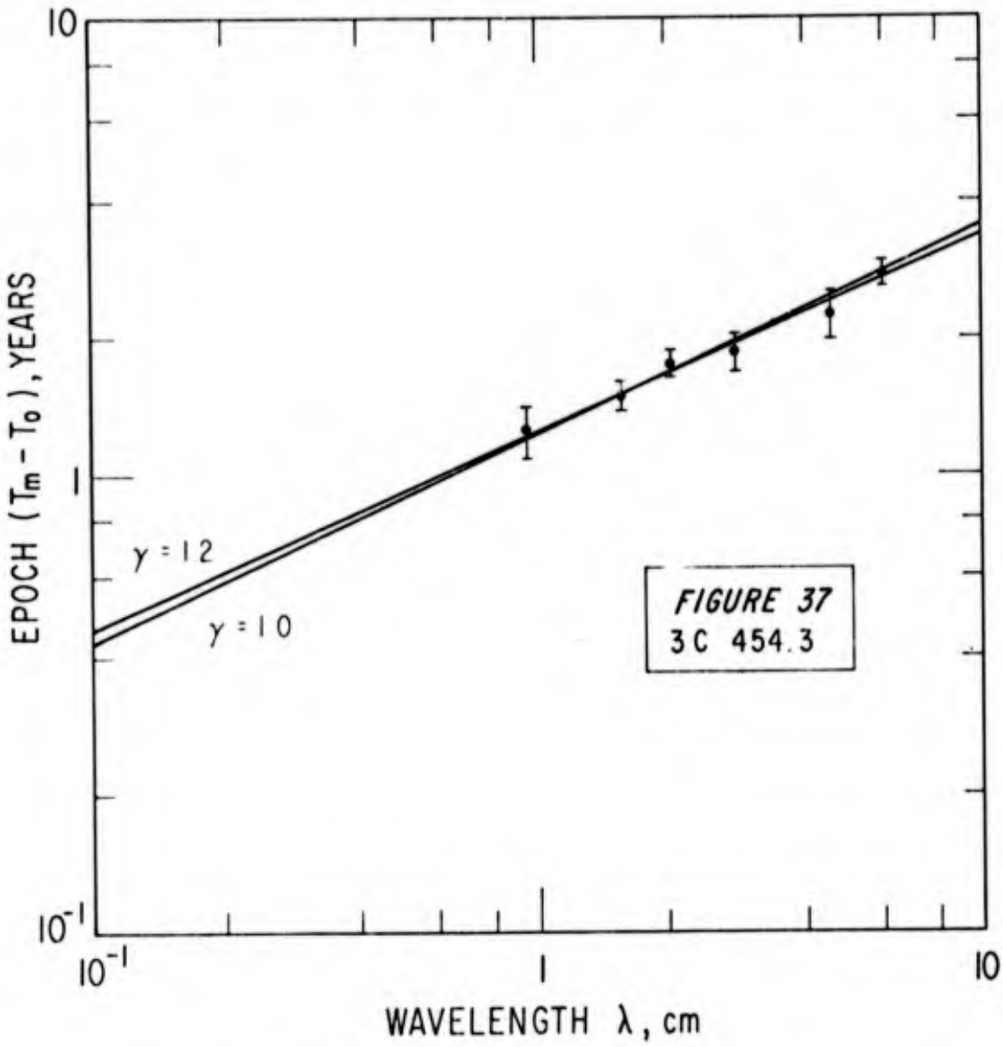
10
1
10^{-1}
10^{-1}
1
10
EPOCH ($T_m - T_o$), YEARS
WAVELENGTH λ, cm
γ = 12
γ = 10
FIGURE 37
3C 454.3

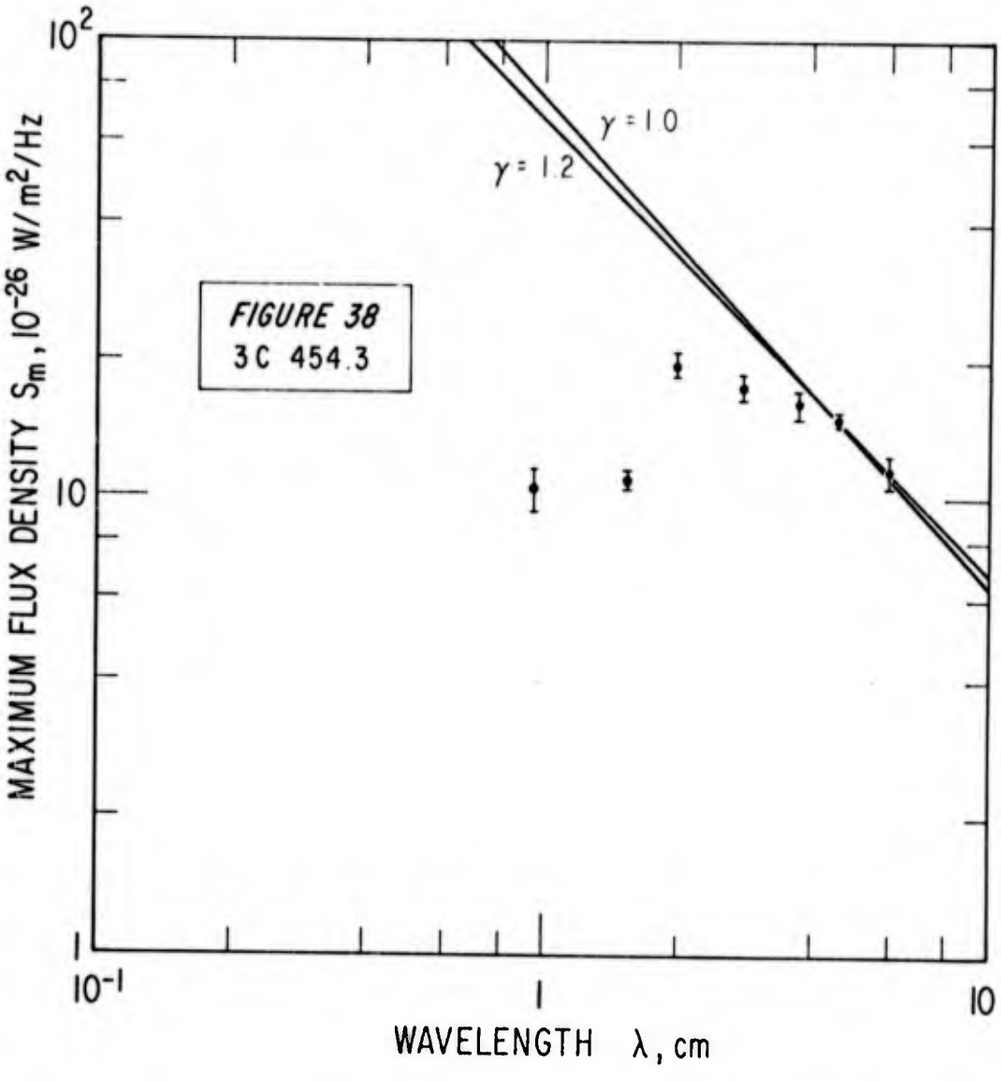
10^2
10
1
10^{-1}
1
10
$\gamma = 1.0$
$\gamma = 1.2$
FIGURE 38
3C 454.3
MAXIMUM FLUX DENSITY S_m, 10^{-26} W/m^2/Hz
WAVELENGTH λ, cm

Only the lowest frequency data fit the prediction of the model.

At the time of the maximum flux density at 2.8 cm the maximum linear extent of the source was 1.86 light years (Maximum angular size of 0.0001 arc sec). The maximum magnetic field strength at this stage of the evolution was 1.2×10^{-6} gauss.

As shown in Fig. 37, the predicted variations of t_m with λ is in excellent agreement with the observations. The correlation between prediction and data for this variation of S_m with λ (Fig. 38) is, however, very poor. In addition, the attempts to form a useful spectra for the event were unsuccessful. The result was only a random scatter of points. Because of the excellent correlation shown in Fig. 37, the model may still partially apply. The S_m vs λ and S vs ν failures may be due to the interaction of later events which tend to confuse the data, as seen in Fig. 35. In addition, the operation of other energy loss mechanisms that dominate over the energy lost in the expansion would lead to this type of failure, i.e., values of S_m lower than predicted. If other energy loss mechanisms such as synchrotron radiation loss and inverse compton scattering are the cause of the lower values of S_m then these processes dominate until the expansion reaches the point where the optical transparence occurs at 4.6 cm.

V. Summary and Conclusions

In the preceeding section the predicted variations of t_m with λ, S_m with λ, and S with ν are shown as slopes superimposed on the observed data. While it is true that in many cases a number of different slopes can be drawn through the data points, the significant fact is, in each case, with one exception, that the one slope predicted by the model does, indeed, fit the data.

Table 1 is a summary of the parameters found and the extent of correlation of the model to the data for the eight events analyzed. The values found for the maximum magnetic field strength are, with the possible exceptions of event III of 3C84 and event I of 3C273, consistent with the assumed upper limit of $\sim 10^{-3}$ gauss. The event in 3C454.3 is the only one which does not completely follow the behavior predicted by the model. Even in this case the model is successful in matching the observed variation of t_m with λ. (Each object analyzed showed its own degree of correlation with the model.) In 3C273 and possibly 3C84 a crossover in time of the manifestations of two events are seen.

The model of a radially expanding sphere of relativistic electrons emitting synchrotron radiation and synchrotron self-absorbed below some crtical frequency does, with the exception noted, satisfactorily explain the observations of seven of the eight event analyzed (Table 1).

TABLE 1

Summary

	3C 84			3C 120		3C 273		3C 454.3
	EVENT I	EVENT II	EVENT III	EVENT II	EVENT III	EVENT I	EVENT II	EVENT I
S	1.0	0.8	1.0	1.0	1.0	1.0	1.2	1.1
τ_o (years)	1966.4 ±0.04	1966.84 ± 0.04	1967.37 ± 0.05	1967.38 ± 0.04	1968.07 ± 0.02	1963.42 ± 0.01	1965.82 ± 0.02	1965.84 ± 0.06
γ	1.0 ± 0.1	1.5 ± 0.1	1.1 ± 0.1	1.0 ± 0.1	1.2 ± 0.1	1.3 ± 0.1	1.6 ± 0.1	1.1 ± 0.1
Correlation of eq.(40) with data	Excellent	Good	Excellent	Excellent	Good	Excellent	Excellent	Excellent
Correlation of eq. (37) with data	Excellent	Excellent	Excellent	Excellent	Good	Excellent	Good	Poor
Correlation of eq.(35)& (36)with data	Excellent	Excellent	———	Excellent	Excellent	———	Good	———
l_{max} (light mos.)	4.2	2.9	3.1	6.4	6.8	72	10.6	22.3
θ (arc sec)	4.15×10^{-4}	2.85×10^{-4}	3.08×10^{-4}	3.4×10^{-4}	3.65×10^{-4}	8.2×10^{-4}	1.2×10^{-4}	1.2×10^{-4}
B_{max} (gauss)	2×10^{-5}	3.6×10^{-4}	4.8×10^{-3}	1.3×10^{-4}	1.7×10^{-4}	9.5×10^{-3}	6.7×10^{-7}	1.2×10^{-6}

The dominant deviations from the model seem to be in the assumed amount of energy loss of the electrons early in the life of the source. (In cases where the maximum flux density is too low to fit the predictions of the model, no change in the assumed quiescent level could be made that would account for it.)

A desirable extension of this work would be the anlysis of additional QSS and refinement of the model to include consideration of energy loss mechanisms other than the expansion, such as synchrotron radiation losses and inverse compton scattering losses. An extension of this work could also include the possibility of continuous or recurring injection of electrons, which would make the value of γ vary with time. In addition, an analysis of the quiescent component to determine if the radiation is synchrotron or thermal would be desirable. Since the value for γ for thermal radiation is negative and for non-thermal processes is zero or positive, a determination of γ from the quiescent spectrum would yield some insight into this question. It has been suggested that the many small outbursts seen at 3.3 mm may contribute to a change in the quiescent level at lower frequencies. The investigation of this possible effect may prove worthwhile.

Bibliography

1. Andrew, B.H., MacLeod,J.M., Locke,J.L., Medd,W.J. "Rapid Radio Variations in BL Lac." Nature, 223:598-599 (July 1969).

2. Burbidge,G.R., Burbidge,E.M. "Red-shifts of Quasi-stellar Objects and Related Extragalactic Systems." Nature, 222:735-741 (may 1969).

3. Dent,W.A. "Variations in the Radio Emission from the Seyfert Galaxy NGC 1275." The Astrophysical Journal, 144:843-846 (February 1966).

4. Dent,W.A. "The 1966-2967 Radio Outburst in 3C 273." The Astrophysical Journal, 153:L29-L32 (July 1968).

5. Dent,W.A. "Quasi-stellar sources: Variations in the Radio Emission of 3C 273." Science, 148:1458-1460 (April 1965).

6. Dent,W.A., Haddock,F.T. "The Extension of Non-Thermal Radio-Source Spectra to 8000 MC/S." The Astrophysical Journal, 144:568-586 (November 1966).

7. Doherty,L.H., MacLeod,J.M., Purton,C.R. "Flux Densities of Radio Sources at a Wavelength of 2.8 cm." The Astronomical Journal, 74:827-832 (August 1969).

8. Dworetsky,M.M., Epstein,E.E., Fogarty,W.G., Montgomery,J.W. "Sagittarius A: Observations of the Galactic Center at 3.3 mm." The Astrophysical Journal, 158 (December 1969).

9. Epstein,E.E. "3.4-MM Observations of the Quasi-Stellar Radio Source #3C 279." The Astrophysical Journal, 142:1282-1285 (June 1965).

10. Epstein,E.E. "On Small-Scale Distribution at 3.4 mm Wavelength of the Reported 3°K Background Radiation." The Astrophysical Journal, 148:L157-L159 (June 1967).

11. Epstein,E.E., Oliver,J.P., Sater,S.L. "Quasi-Stellar Radio Sources: 88 GHz Flux Measurements." The Astrophysical Journal, 151:L27-L31 (January 1968).

12. Ginzberg,V.L., Syrovatskii,S.I. "Cosmic Magneto-bremsstrahlung (Synchrotron Radiation)." Annual Review of Astronomy and Astrophysics, 3:297-350 (1965).

13. Hobbs,R.W., Corbett,H.H., Santini,N.J. "Observations

of Radio Sources at 4.3-mm Wavelength." The Astronomical Journal, 74:824-826 (August 1969).

14. Hobbs,R.W., Corbett,H.H., Santini,N.J. "Observations of Variable Radio Sources at 9.55 Millimeter Wavelength." The Astrophysical Journal, 156:L15-L18 (February 1969).

15. Hobbs,R.W. (Private Communication) 1969.

16. Hornby,J.M., Williams,P.J.S. "Radio Sources Having Spectra with a Low Frequency Cut-off." Monthly Notice of the Royal Astronomical Society, 131:237-246 (June 1966).

17. Kellerman,K.I. "On the Interpretation of Radio-Source Spectra and the Evaluation of Radio Galaxies and Quasi-Stellar Sources." The Astrophysical Journal, 146:621-633 (December 1966).

18. Kellerman,K.I., Pauliny-Toth,I.I.K. "The Spectra of Opaque Radio Sources." The Astrophysical Journal, 155:L71-L78 (December 1969).

19. Kellerman,K.I., Pauliny-Toth,I.I.K. "Variable Radio Sources." Annual Review of Astronomy and Astrophysics, 6:417-488 (1968).

20. Kellerman,K.I., Pauliy-Toth,I.I.K., Tyler,W.C. "Measurements of the Flux Density of Discrete Radio Sources at Centimeter Wavelengths. I. Observations at 2695 MHz (11.3 cm)." The Astronomical Journal, 73: 298-309 (June 1968).

21. Kinman,T.D. "Optical Polarization Measures of Five Radio Sources." The Astrophysical Journal, 148:L53-L56 (May 1967).

22. Kraus,J.D. Radio Astronomy. New York McGraw-Hill 1966.

23. LeRoux,E. "Etude Theorique de Rayonnment Synchrotron des Radiosources." Annales d'Astrophysiques, 24:71-85 (December 1961).

24. Locke,J.L. (Private Communication) 1969.

25. Locke,J.L., Andrew,B.H., Medd,W.J. "Three Radio Sources with Unusual Intensity Variations." The Astrophysical Journal, 157:L81-L86 (August 1969).

26. McCullogh,T.P., Waak,J.A. "Intensity and Polarization Measurements of Variable Sources at 1.55 CM Wavelengths." The Astrophysical Journal (in print).

27. Medd,W.J., Locke,J.L., Andrew,B.H., Van Den Bergh, S. "Observations of Variable Radio Sources at 2.8 cm." The Astronomical Journal, 73:293-297 (June 1968).

28. Oster,L. "New Restriction on Models for Quasi-Stellar Objects." Advanced Research Projects Agency. University of Colorado (January 1968).

29. Pacholczyk,A.G. Radio Astrophysics. In Print.

30. Pacholczyk,A.G., Weyman,R., Editors. "Proceedings of the Conference on Seyfert Galaxies and Related Objects, Held at Steward Observatory, University of Arizona." The Astronomical Journal, 73:836-943 (February 1968).

31. Pauliny-Toth,I.I.K. (Private Communication) 1969.

32. Pauliny-Toth,I.I.K, Kellerman,K.I. "Measurements of the Flux Density and Spectra of Discrete Radio Sources at Centimeter Wavelengths. II. The Observations at 5 GHz (6 cm)." The Astronomical Journal, 73: 953-968 (December 1968).

33. Pauliny-Toth,I.I.K., Kellerman,K.I. "Variations of the Radio-Frequencie Spectra of 3C 273, 3C 279, and Other Radio Sources." The Astrophysical Journal, 146:634-645 (June 1966).

34. Pauliny-Toth,I.I.K., Kellerman,K.I. "Repeated Outbursts in the Radio Galaxie 3C 120." The Astrophysical Journal, 152:L169-L175 (June 1968).

35. Rees,M.F. "A Relativistically Expanding Model for Variable Quasi-Stellar Radio Sources." Monthly Notice of the Royal Astronomical Society, 135:345-360 (September 1967).

36. Shimabukuro,F.I., Epstein,E.E. "Attenuation and Emission of the Atmosphere at 3.3 mm." IEEE Transactions on Antenna and Propogation In Press.

37. Shklovskii,I.S. "Secular Variation of the Flux and Intensity of Radio Emission from Discrete Sources." Astronomicheskii Zhurnal, 37:256-264 (March 1960).

38. Shklovskii,I.S. "Possible Secular Variation of the Flux and Spectrum of Radio Emission of Source

1934-63." Nature, 296:176-177 (April 1965).

39. Simon,M. "Particle Acceleration During the 1966-67 Radio Outburst of 3C 273." Report (June 1969).

40. Simon,M. "Asymptotic Form for Synchrotron Spectra Below Razin Cutoff." The Astrophysical Journal, 156: 341-344 (April 1969).

41. Slish,V.I. "Angular Size of Radio Stars." Nature, 199:682 (August 1963).

42. Stein,W.A. "The Millimeter Radiation from 3C 273." The Astrophysical Journal, 148:689-694 (June 1967).

43. Sturrock,P.A. Accelaration on a Galactic Scale. Defense Documentation Center, Stanford University (May 1967).

44. Sturrock,P.A., Feldman,P.A. "A Mechanism for Quasar Continuum Radiation, With Application to 3C 273B." SU-IPR Report No. 215. Office of Naval Research Contract. (December 1967).

45. Terrell,J. "Quasi-Stellar Diameters and Intensity Fluctuations." Science, 145:918-919 (August 1964).

46. van der Laan,M. "Radio Galaxies." Monthly Notice of the Royal Astronomical Society, 126:519-533 (May 1964).

47. van der Laan,M. "A Model for Variable Extragalactic Radio Sources." Nature, 211: 1131 (July 1966).

48. Williams,P.J.S. "Absorption in Radio Sources of High Temperature." Nature, 200:56-57 (September 1963).

49. Waak,J.A. (Private Communication) 1969.

50. Woltjer,L Discussions of Observations of Quasi-Stellar Sources, Radio Galaxies and Supernova Remnants. Columbia University.

51. Woltjer,L. "Inverse Compton Radiation in Quasi-Stellar Objects." The Astrophysical Journal, 146: 597-599 (November 1966).

Appendix A

Attenuation of a Wave Propogating in an Absorbing Medium

Consider a wave propogating in an absorbing medium. The flux density of the wave will decrease an amount dS in a distance dx given by:

$$dS = -S\alpha\, dx \tag{A-1}$$

where S = flux density at point x

dS = decrease in flux density

α = attenuation constant

dx = element of length

Dividing by S and integrating yields:

$$\int \frac{dS}{S} = -\int \alpha\, dx \tag{A-2}$$

$$\ln S = -\alpha x + C \tag{A-3}$$

At the boundary of the medium (x = 0) the flux density is S_o, thus:

$$\ln S_o = C \tag{A-4}$$

and (3) becomes:

$$\ln \frac{S}{S_o} = -\alpha x \tag{A-5}$$

or

$$S = S_o e^{-\alpha x} \tag{A-6}$$

Define the optical depth $\tau \equiv \alpha x$ (A-7)

where x is the thickness of the absorbing medium. If we measure the angle, z, from the normal to the medium, then

the total optical depth is now expressed as $\tau \sec z$. Therefore:

$$S = S_o e^{-\tau \sec z} \tag{A-8}$$

where x is now the thickness of the absorbing medium at $z = 0^o$.

Since flux density is directly proportional to antenna temperature, equation (A-8) can be expressed as;

$$T_a' = T_a e^{-\tau \sec z} \tag{A-9}$$

Appendix B

Internal Emission and Absorption of a Medium With an Emission Coefficient

Consider an element of volume dv of matter. The power per unit bandwidth emitted by the volume is then

$$dw = j\rho dv \tag{B-1}$$

where dw = power emitted per unit bandwidth

j = emission coefficient

ρ = density

The flux density dS observed at a distance r is

$$dS = \frac{dw}{4\pi r^2} = \frac{j\rho dv}{4\pi r^2} \tag{B-2}$$

while the intensity dI is

$$dI = \frac{dS}{d\Omega} = \frac{j\rho dv}{4\pi r^2 d\Omega} \tag{B-3}$$

where $d\Omega$ = element of solid angle. Since the volume $dv = r^2 dr\, d\Omega$, this reduces to

$$dI = \frac{j\rho dr}{4\pi} \tag{B-4}$$

Absorption between dv and the edge of the medium will result in attenuation of an amount $e^{-\tau}$ (from Appendix A). Thus, the infinitesimal intensity received outside the absorbing medium due to emission by the volume dv is

$$dI = \frac{1}{4\pi}\, j\rho dr e^{-\tau} \tag{B-5}$$

Introducing K, the volume absorption coefficient which is defined by

$$\tau \equiv \int_o^r K\rho dr \tag{B-6}$$

$$dI = \frac{1}{4\pi K} e^{-\tau} K\rho dr \tag{B-7}$$

Integrating yields

$$I = \frac{1}{4\pi K} \int_o^r e^{-\tau} K\rho dr = \frac{1}{4\pi K} \int_o^\tau e^{-\tau} d\tau = \frac{1}{4\pi K} \left(1-e^{-\tau}\right) \tag{B-8}$$

As τ increases I approaches $\frac{1}{4\pi K}$, which may be regarded as the intrinsic intensity I_o of the medium. Thus

$$I = I_o \left(1-e^{-\tau}\right) \tag{B-9}$$

where I = apparent or observed intensity

I_o = intrinsic intensity

τ = optical depth

At radio frequencies the intensity is proportional to temperature (from the Rayleigh-Jeans law). Hence

$$T = T_o \left(1-e^{-\tau}\right) \tag{B-10}$$

or, using sec z as defined previously,

$$T = T_o \left(1-e^{-\tau \sec z}\right) \tag{B-11}$$

Combining both attenuation of external radiation (eq. A-9) with the internal emission and absorption (eq. B-11) yield

$$T_a' = T_a e^{-\tau \sec z} + T_o \left(1-e^{-\tau \sec z}\right) \tag{B-12}$$

Vita

Gordon Derossi was born on [redacted], in [redacted] New York. He graduated from Samuel Gompers Vocational and Technical High School in June, 1959. After completing his sophmore year at Long Island University, he enlisted in the Air Force in February, 1963. Through the Airman's Education and Commissioning Program he received a Bachelor of Science degree from the University of Wyoming at Laramie in June, 1966. He received his reserve commission in the Air Force in September, 1966, after completeing Officer Training School and received a regular commission in October, 1969. Prior to entering the Air Force Institute of Technology in August, 1968, he was a launch control officer in the Air Force Systems Command Thor Agena Program Office at Vandenberg Air Force Base, California.

[redacted]

Unclassified
Security Classification

DOCUMENT CONTROL DATA - R & D

(Security classification of title, body of abstract and indexing annotation must be entered when the overall report is classified)

1. ORIGINATING ACTIVITY (Corporate author)
Air Force Institute of Technology (AFIT-SE)
Wright-Patterson AFB, Ohio 45433

2a. REPORT SECURITY CLASSIFICATION
Unclassified

2b. GROUP

3. REPORT TITLE
A Test of the Synchrotron Expanding Source Model of Quasi-Stellar Radio Source Variations

4. DESCRIPTIVE NOTES (Type of report and inclusive dates)
AFIT Thesis

5. AUTHOR(S) (First name, middle initial, last name)
Gordon Derossi
Captain USAF

6. REPORT DATE
June 1970

7a. TOTAL NO. OF PAGES
95

7b. NO. OF REFS
51

8a. CONTRACT OR GRANT NO.

b. PROJECT NO.
N/A

c.

d.

9a. ORIGINATOR'S REPORT NUMBER(S)
GSP/PH/70-6

9b. OTHER REPORT NO(S) (Any other numbers that may be assigned this report)

10. DISTRIBUTION STATEMENT This document is subject to special export controls and each transmittal to foreign governments or foreign nationals may be made only with prior approval of the Dean of Engineering, Air Force Institute of Technology, Wright-Patterson Air Force Base, Ohio, 45433

11. SUPPLEMENTARY NOTES

12. SPONSORING MILITARY ACTIVITY

13. ABSTRACT

The validity of the synchrotron expanding source model for quasars as proposed by Shklovskii, Kellerman and van der Laan is tested, using observations of the radio emission from four quasi-stellar radio sources. The time dependence of the recorded variations of radio emission in the range from 3.3 mm to approximately 6 cm, taken during the period from 1965 to late 1969 from QSS 3C84, 3C120, 3C273 and 3C454.3 is compared to the time dependence of the variations predicted by the proposed model. Correlation between observed variations and predicted variations is excellent in over 85% of the cases tested.

DD FORM 1 NOV 65 1473

Unclassified
Security Classification

Security Classification

14 KEY WORDS	LINK A		LINK B		LINK C	
	ROLE	WT	ROLE	WT	ROLE	WT
Quasi-Stellar Radio Source						
Quasar						
Synchrotron Radiation						
Radio Astronomy						
Cosmology						
Celestial Radio Source Variations						
Extra-galactic Millimeter radiation						

Unclassified
Security Classification